scientific reports

Check for updates

OPEN

Effects of NAD+ repletion with Nicotinamide riboside on obesity-induced chronic kidney disease and renal cell lipotoxicity

Morgane Decarnoncle[1,4], Louise Pierre[1,2,4], Marine Thirion[1], Hélène Marlier[1,2], Louis Maréchal[1,2], Pauline Rouzé[1], Inès Jadot[3], Thierry Arnould[2], Anne-Emilie Declèves[1] & Florian Juszczak[1]✉

Nicotinamide riboside (NR), a natural precursor of NAD+, has been suggested to confer protection against metabolic and age-related disorders. However, its effect on chronic kidney disease (CKD), particularly in the context of obesity, remains poorly understood. Here, we evaluated the potential effects of NR supplementation in models of obesity-induced renal injury. The metabolic and renal effects of both preventive and interventional NR supplementation were assessed in mice fed high-fat or low-fat diets. Our data showed that NAD+ repletion by NR supplementation, whether preventive or interventional, did not affect body or organ weights, and did not ameliorate glucose metabolism, insulin resistance, or hepatic and renal lipid accumulation. NR supplementation was however associated with SIRT3-mediated deacetylation of SOD2 in the renal tissue of obese mice. It moderately reduced renal dysfunction and was associated with increased mitochondrial content. To further explore the cellular mechanisms underlying the renal effects of NR in a lipotoxic context, we investigated its impact on renal proximal tubular cells exposed to palmitic acid (PA). NR significantly prevented oxidative stress in proximal tubular epithelial cells, as evidenced by the activation of SOD2 as well as the reduction of lipid peroxidation. Moreover, NR improved mitochondrial damage and promoted mitophagy. However, NR did not reduce PA-induced lipid accumulation. In conclusion, this study provides evidence that NR exerts antioxidant effects and enhances mitochondrial function in renal cells in vitro but does not protect obese mice from metabolic disorders and associated CKD.

Keywords Nicotinamide riboside, Obesity, High-fat diet, Renal function, Kidney disease, Oxidative stress

In recent decades, obesity has escalated into a global epidemic, driven primarily by sedentary lifestyles and high-calorie diets[1]. Obesity is a well-established risk factor for several comorbidities including abdominal adiposity, hyperlipidemia, hyperglycemia, hyperinsulinemia, and hypertension, which collectively contribute to the development of chronic diseases such as MASLD (metabolic dysfunction-associated steatotic liver disease), type 2 diabetes and cardiovascular disease[2]. Particularly, obesity is also a significant risk factor for chronic kidney disease (CKD) and a strong predictor for the progression to end-stage renal disease (ESRD)[3]. Obesity-induced CKD is characterized by specific pathological changes including obesity-related glomerulopathy, defined by glomeruli enlargement, hypertension and hyperfiltration which may lead to the development of focal segmental glomerulosclerosis[4]. These structural changes impair kidney function over time. Additionally, in rodents and humans, obesity has been shown to promote ectopic lipid accumulation in renal cells and particularly in proximal tubular epithelial cells (PTECs)[5–9]. This lipid accumulation disrupts normal lipid metabolism by inhibiting fatty acid oxidation (FAO) and activating lipogenesis. Overall, abnormal lipid metabolism in the kidneys has been shown to impair cell function and contribute to renal damage and CKD development[5–9]. Moreover, evidence

[1]Laboratory of Metabolic and Molecular Biochemistry, Faculty of Medicine, Pharmacy and Biomedical Sciences (FMPB), Research Institute for Health Sciences and Technology, University of Mons (UMONS), Avenue du Champ de Mars, 6, 7000 Mons, Belgium. [2]Biochemistry and Cellular Biology Research Unit (URBC), Namur Research Institute for Life Sciences (NARILIS), University of Namur (UNamur), 5000 Namur, Belgium. [3]Molecular Physiology Research Unit (URPhyM), Namur Research Institute for Life Sciences (NARILIS), University of Namur (UNamur), 5000 Namur, Belgium. [4]Morgane Decarnoncle and Louise Pierre contributed equally to this work. ✉email: Florian.juszczak@umons.ac.be

suggests that obesity disrupts mitochondrial function and increases oxidative stress in PTECs, contributing to renal damage[10]. Particularly, these cells primarily rely on free fatty acids as an energy source, which are catabolized through mitochondrial FAO and oxidative phosphorylation (OXPHOS). Impaired mitochondrial function in PTECs leads to increased production of reactive oxygen species (ROS), which damage cellular components and promote inflammation[11].

Despite extensive efforts to develop therapeutic strategies for obesity-related CKD, effective treatments remain limited, often accompanied by significant side effects. This highlights the urgent need for alternative therapies. Among them, those protecting kidney cells by supporting mitochondrial function and reducing oxidative stress seem to offer the potential to slow down the progression of kidney disease in obese individuals[12]. Recently, studies have demonstrated that nicotinamide adenine dinucleotide (NAD^+) metabolism is disturbed in human kidneys as well as in animal models with CKD[13–15]. NAD^+ is a coenzyme that plays a crucial role in mitochondrial ATP production and oxidative reactions. It also serves as a co-substrate for NAD^+-dependent deacetylases, such as sirtuins, or consumed by PARPs (poly-ADP ribose polymerases) involved in DNA damage repair. Sirtuins regulate many key metabolic processes involved in maintaining cellular redox balance and mitochondrial integrity, including anti-oxidative response, mitochondrial biogenesis, mitochondrial dynamics and mitophagy[16]. Particularly, sirtuin 3 (SIRT3) deacetylates and activates superoxide dismutase 2 (SOD2), a critical enzyme that mitigates oxidative damage by converting superoxide radicals into hydrogen peroxide and molecular oxygen[17]. SIRT3 enhances the activity of SOD2 through deacetylation of specific lysine residues (such as K68 and K122)[17–19]. Mice deficient in quinolinate phosphoribosyltransferase (QPRT), an enzyme essential for de novo NAD^+ biosynthesis, showed increased susceptibility to acute kidney injury (AKI)[14]. During AKI, both NAD^+ consumption and synthesis are disrupted, leading to impaired FAO, ectopic lipid accumulation within the kidney, and tubular dysfunction[20]. Additionally, diabetic kidney disease (DKD) is linked to a reduction in the intrarenal NAD^+/NADH ratio, which contributes to mitochondrial oxidative stress[21]. These findings highlight the critical role of NAD^+ in maintaining kidney function, particularly under conditions of stress such as AKI and DKD. While NAD^+ depletion is linked to a wide spectrum of pathological conditions including neurological and age-related disorders, studies indicate that restoring NAD^+ levels with precursors may alleviate these pathological conditions, potentially by supporting redox balance and mitochondrial function during cellular stress and injury[22]. Nicotinamide Riboside (NR) is a form of vitamin B3 and a naturally occurring precursor of NAD^+, found in sources such as cow's milk[23]. NR is converted to NAD^+ primarily via the NR kinase (NRK) pathway[24,25]. In mice and humans, NR treatment has been shown to be more efficient in boosting NAD^+ than other NAD^+ precursors such as Nicotinic Acid (NA) or Nicotinamide (NAM)[26]. Several studies have shown that NR supplementation increases NAD^+ level, enhances mitochondrial biogenesis and oxidative metabolism, and thus protects against neurodegenerative disorders and age-related physiological decline in mammals[27]. In their study, Canto and colleagues demonstrated that NR treatment at a dose of 400 mg/kg/day for 10 weeks in high-fat diet (HFD)-fed mice increased plasma and intracellular NAD^+ levels in muscles, brown adipose tissue, and liver. NR supplementation also enhanced SIRT3-mediated SOD2 deacetylation in cultured cells and in the muscle tissue, which improved mitochondrial function and oxidative capacity[28].

The effects of NR supplementation on the renal tissue and obesity-associated kidney dysfunction are still unknown. This study investigated the effects of NR treatment in obese mice with CKD as well as in PTECs in conditions of lipotoxicity. We showed that, in vitro, NR supplementation reduces oxidative stress and enhances mitochondrial function in PTECs. However, in vivo, it does not prevent renal dysfunction and instead induces lipid accumulation in both the kidney and liver, particularly with long-term supplementation.

Results

Preventive or interventional NR supplementation does not affect metabolic syndrome parameters

We investigated the effect of early and late NR supplementation in low-fat diet (LFD)- or high-fat diet (HFD)-fed mice. NR was administered either concomitantly with the diet (LFD NR20 and HFD NR20) or as an interventional treatment during the last 8 weeks of the protocol (LFD NR8 and HFD NR8) (Fig. 1a). Indeed, obese mice fed a HFD for at least 12 weeks are known to develop characteristic features of obesity-related nephropathy[29]. The data presented in Fig. 1b indicates that when comparing mice fed a HFD to those fed a LFD, there was a significant increase in body weight starting from week 8. However, when comparing mice within the same dietary groups, no significant differences in body weight were observed in response to NR supplementation. Moreover, the weights of liver, kidney and heart were significantly higher ($P\_diet < 0.001$) in all HFD-fed mice groups compared with LFD-fed mice groups at week 20 (Fig. 1c-e). In accordance with previous reports, mice fed a HFD for 20 weeks developed glucose intolerance, hyperglycemia, and hyperinsulinemia[8]. Results of the glucose tolerance tests (GTTs) at week 0, 12 and 20 confirmed the development of glucose intolerance in all HFD animals and the absence of NR supplementation effect (Fig. 2a-c). Moreover, the glycemia and insulinemia were significantly higher ($P\_diet < 0.001$) in all HFD groups compared to LFD groups with no significant effect of preventive or interventional NR supplementation (Fig. 2d, e). The calculation of the HOMA-IR (Homeostatic Model Assessment for Insulin Resistance), an indicator of insulin resistance, demonstrated that NR supplementation does not significantly alter IR in HFD mice (Fig. 2f). Altogether, these results show that NR has no influence on impaired glucose metabolism and insulin resistance in obese mice. The total plasma concentrations of cholesterol were also measured in each experimental group as another indicator of the metabolic syndrome. As illustrated in Fig. 2g, HFD induced a significant elevation of plasma cholesterol levels, whereas this increase was counteracted only in the HFD NR20 group when compared to HFD. Furthermore, we investigated plasma interleukin 6 (IL-6) as a circulating marker of systemic inflammation and the data reported an increased concentration of this proinflammatory cytokine in the plasma of HFD mice that was not significantly reduced with NR (Fig. 2h).

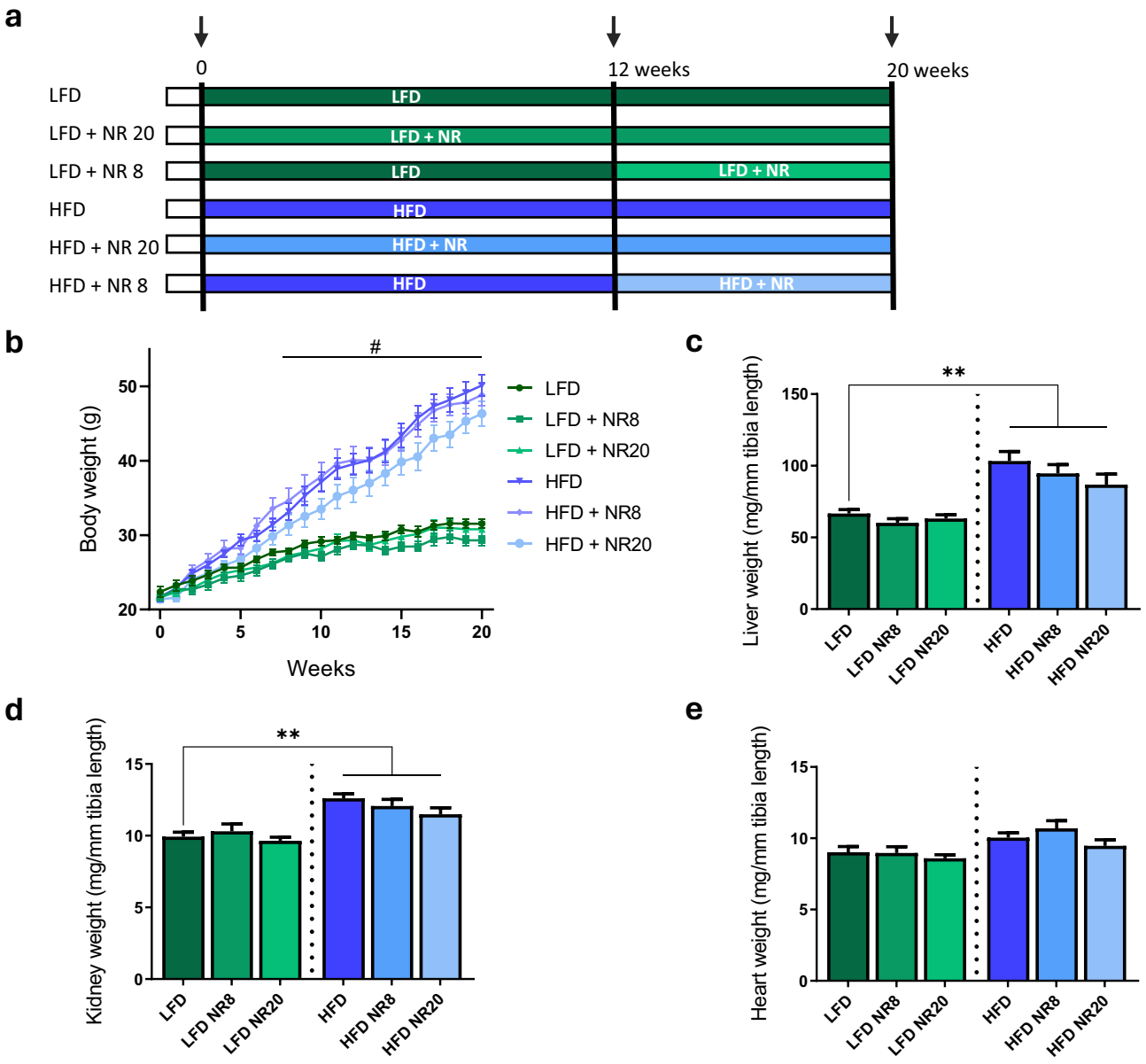

Fig. 1. Preventive or interventional NR supplementation did not impact body nor organ weights in mice fed with low- or high-fat diet. **(a)** Schematic representation of experimental design. Eight-weeks old C57Bl6/J male mice were randomized to either a low- (LFD) or high-fat diet (HFD) supplemented or not with 400 mg/kg/Day of nicotinamide riboside (NR) from week 0 (preventive) or week 12 (interventional) for a total of 20 weeks. At week 0, 12, and 20 (represented by black arrows), urine collection and GTTs were performed. **(b)** Body weight evolution over time of LFD or HFD animals supplemented or not with NR. **(c-e)** Measurements of the **(c)** liver, **(d)** kidney, and **(e)** heart weights at week 20 in LFD or HFD animals supplemented or not with NR. Data are presented as means ± SEM, n = 10 in each group. Statistical analyses were performed by two-way ANOVA followed by Sidak's post hoc test. $^{\#}p \leq 0.05$ between LFD and HFD groups; $^{*}p \leq 0.05$; $^{**}p \leq 0.01$ between groups.

NR supplementation does not improve hepatic steatosis in obese mice but reduces liver fibrosis

HFD-fed mice exhibited features of hepatic steatosis, characterized by substantial lipid droplet (LD) accumulation within hepatocytes (Fig. 3a, b). Notably, NR supplementation did not alleviate hepatic lipid accumulation in HFD-fed mice but significantly increased steatosis (P_treatment < 0.01). Particularly, moderate LD accumulation was observed in hepatocytes of LFD animals receiving NR, regardless of the supplementation duration. In addition, hepatic fibrosis was assessed using picrosirius Red staining. As shown in Fig. 3d, liver tissues from HFD-fed mice displayed a significantly higher percentage of fibrosis when compared to the LFD control groups. Interestingly, both early and late NR supplementation effectively prevented the development of liver fibrosis in HFD-fed mice (P_treatment < 0.01). To investigate potential liver injury following NR treatment, we measured

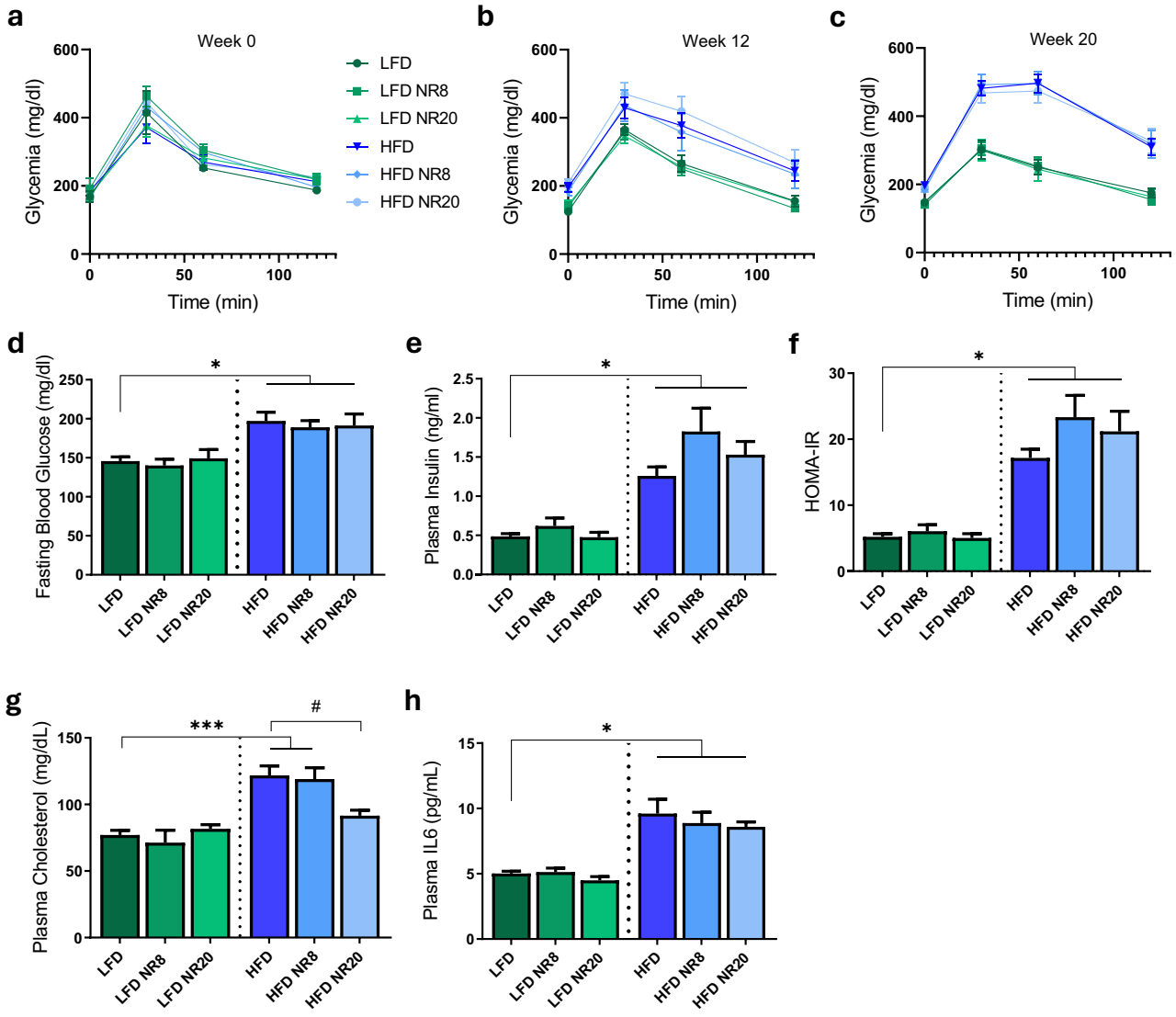

Fig. 2. Preventive or interventional NR supplementation did not improve parameters of the metabolic syndrome. **(a-c)** Glucose tolerance tests of LFD or HFD mice supplemented or not with NR at **(a)** week 0, **(b)** week 12 and **(c)** week 20. Glycemia was measured in fasted mice before (0 min) and 30, 60 and 120 min after intraperitoneal injection of 2 g/kg b.w. glucose. **(d)** Measurement of fasted blood glucose at week 20 in LFD or HFD animals supplemented or not with NR. **(e)** Measurement of plasma insulin at week 20 in LFD or HFD animals supplemented or not with NR. **(f)** HOMA-IR index for LFD or HFD animals supplemented or not with NR after 20 weeks. **(g)** Assessment of plasma cholesterol levels at week 20 in LFD or HFD animals supplemented or not with NR. **(h)** Measurement of plasma IL-6 levels at week 20 in LFD or HFD animals supplemented or not with NR. Data are presented as means ± SEM, n = 10 in each group. Statistical analyses were performed by two-way ANOVA followed by Sidak's post hoc test. *$p \leq 0.05$; ***$p \leq 0.001$; #$p \leq 0.05$ between groups.

serum AST and ALT levels (Fig. 3e, f). As expected, both GOT and GPT were increased in response to the HFD (P_diet < 0.05 and P_diet < 0.01, respectively), consistent with hepatic steatosis. No significant effect of NR treatment was observed under our experimental conditions suggesting no further toxicity with NR exposure.

NR supplementation moderately improves renal function and does not reduce renal lipid accumulation

HFD mice typically exhibit significant alterations in renal function and disturbance in lipid metabolism[7]. HFD is associated with glomerular hypertrophy, mesangial matrix expansion, and a decline in renal function, as evidenced by increased albuminuria[8]. Additionally, LD accumulation is commonly observed in PTECs of HFD-fed animals, reflecting lipid metabolism dysregulation in the kidney[5,7]. Figure 4 illustrates that mice fed a HFD alone developed glomerular hypertrophy as evidenced by an increase (P_diet < 0.05) in mesangial matrix area (Fig. 4a-c). This phenotype is concomitant with renal function decline in HFD animals as they present a

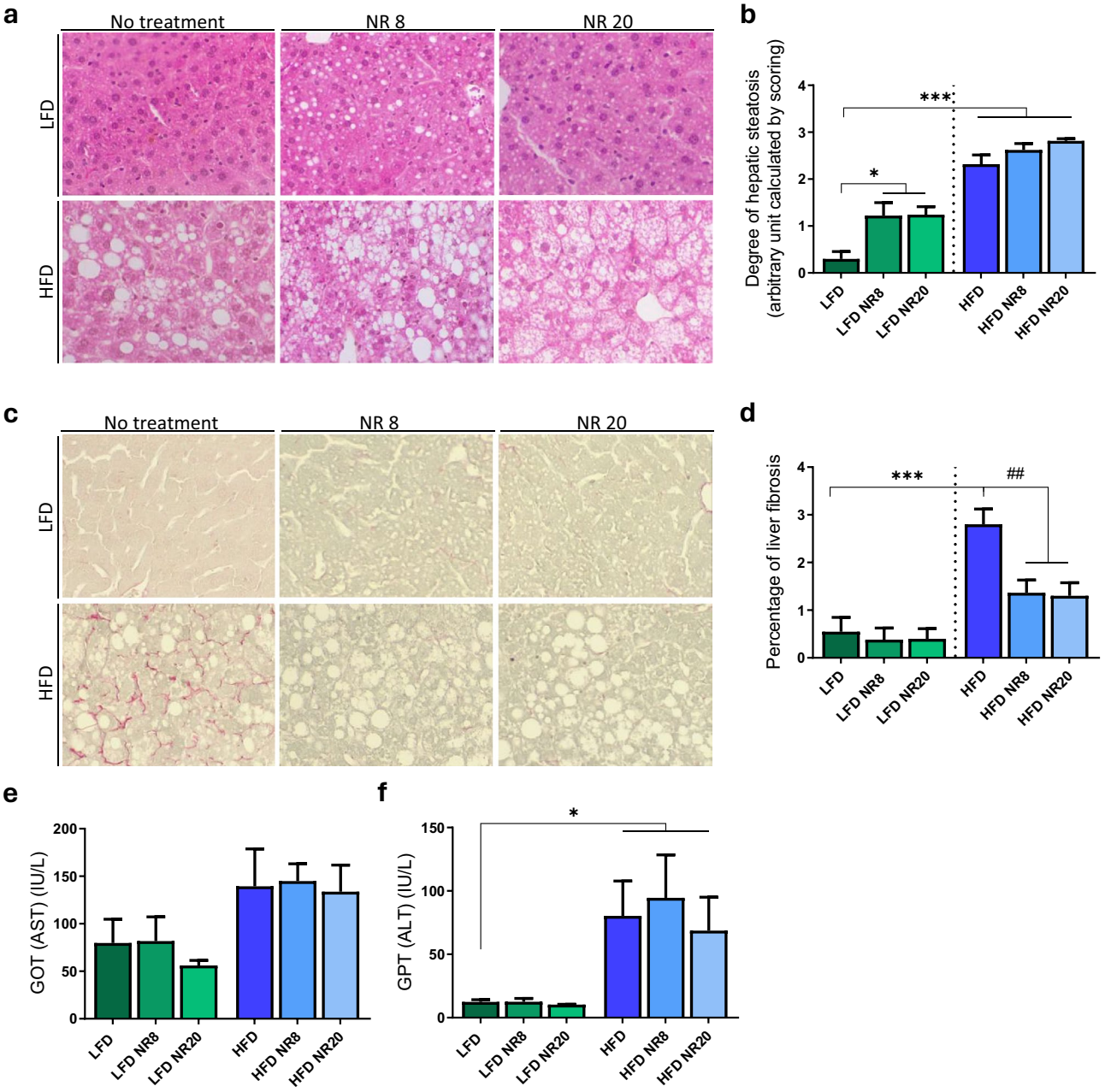

Fig. 3. NR supplementation reduces liver fibrosis but does not improve hepatic steatosis in obese mice. (**a**) Representative photomicrographs of liver sections from LFD or HFD animals supplemented or not with NR at week 20 and stained with hematoxylin and eosin (original magnification ×400). **(b)** Semi-quantitative analysis of hepatic steatosis by scoring. **(c)** Representative photomicrographs of liver sections from LFD or HFD animals supplemented or not with NR at week 20 and stained with picrosirius Red (original magnification ×400). **(d)** Quantitative analysis of the percentages of staining positive for picrosirius red indicative of liver fibrosis. Data are presented as means ± SEM, n = 10 in each group. (e–f) Assessment of plasma GOT and GPT levels at week 20 in LFD or HFD animals supplemented or not with NR. Data are presented as means ± SEM, n = 6 in each group. Statistical analyses were performed by two-way ANOVA followed by Sidak's post hoc test. $^{*}p \leq 0.05$; $^{***}p \leq 0.001$; $^{\#\#}p \leq 0.01$ between groups.

significantly increased albuminuria (Fig. 4d; P_diet < 0.001). Interestingly, in HFD mice supplemented with NR as an interventional treatment, albuminuria is statistically decreased compared to HFD mice, but not when NR is used as a preventive strategy. (Fig. 4d). We also measured BUN, plasma creatinine and cystatin-C. Our data revealed a significant decrease in BUN in both HFD and NR-treated groups (P_diet < 0.05, P_treatment < 0.05), while serum creatinine remained unchanged across conditions, suggesting preserved glomerular filtration (Supp. Figure 1). This pattern could be related to hepatic or systemic regulation of nitrogen metabolism, although it needs to be further investigated. Interestingly, cystatin-C plasmatic levels are decreased in all HFD groups

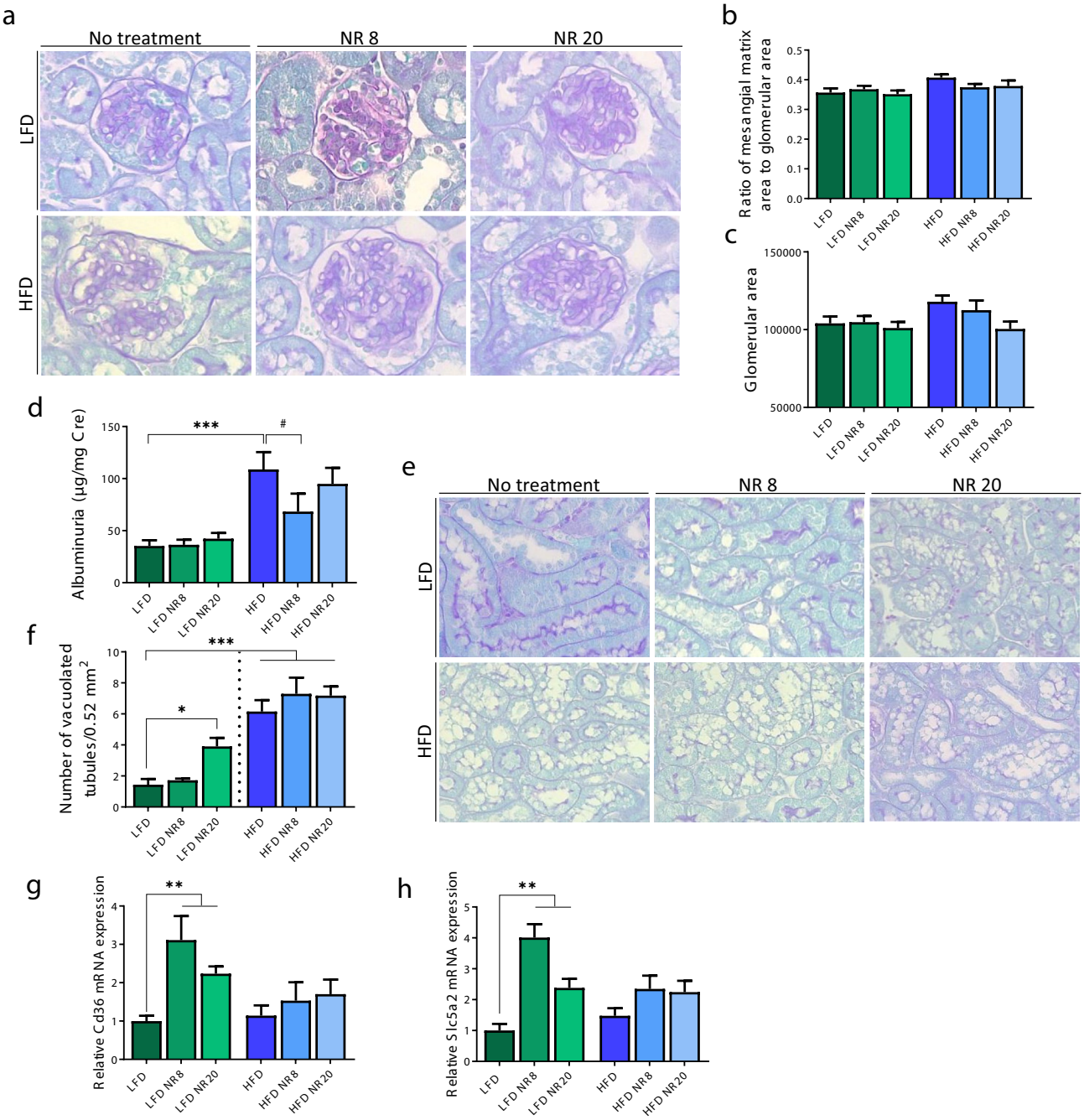

Fig. 4. NR supplementation has limited effects on renal function and does not reduce ectopic lipid accumulation in proximal tubules of obese mice. **(a)** Representative photomicrographs of kidney sections from LFD or HFD animals supplemented or not with NR at week 20 and stained with Periodic Acid Schiff and Luxol Fast Blue (original magnification ×400). **(b, c)** Quantification of the mean ratio of mesangial matrix area to glomerular area and the mean glomerular area from 15 glomeruli per kidney section with one section per animal (arbitrary units). **(d)** Quantitative measurement of the ratio between urinary albumin and urinary creatinine at week 20 in LFD or HFD animals supplemented or not with NR. **(e)** Representative photomicrographs of kidney sections showing tubular vacuolization from LFD or HFD animals supplemented or not with NR at week 20 and stained with Periodic Acid Schiff and Luxol Fast Blue (original magnification ×400). **(f)** Quantitative analysis of number of vacuolated tubules per 0.52 mm^2 of renal section. Data are presented as means ± SEM, n = 10 in each group. **(g-h)**. Relative mRNA expression of *CD36* and Slc5a2 (SGLT2) in the renal cortex from LFD or HFD animals supplemented or not with NR at week 20. Data are presented as means ± SEM, n = 6 in each group. Statistical analyses were performed by two-way ANOVA followed by Sidak's post hoc test. *p ≤ 0.05; **p ≤ 0.01; ***p ≤ 0.001; #p ≤ 0.05 between groups.

compared with LFD groups (P_diet < 0.05), consistent with glomerular hyperfiltration in obese animals while NR treatment had no significant effect. Using Picrosirius Red staining (as done for liver), we demonstrated that renal fibrosis was not affected by either diet or NR supplementation, with no significant differences observed among the different groups (Suppl. Figure 1). We further examined LD accumulation in proximal tubules (Fig. 4e, f). We confirmed the presence of LDs in PTECs from HFD mice (P_diet < 0.001), and the overall effect of NR supplementation further increased LD accumulation in renal tissue (P_treatment < 0.05), similar to what was observed in liver tissue. In particular, LFD group treated with NR for 20 weeks present a moderate, but significantly increased LD accumulation in proximal tubules. To explore potential mechanisms, we assessed the renal expression of CD36 (the major fatty acid transporter in PTECs) and observed a surprising upregulation following NR exposure (Fig. 4g; P_treatment < 0.001). We also measured SGLT2 expression (the transporter involved in glucose reabsorption in PTECs) which was similarly increased (Fig. 4h; P_treatment < 0.0001). These results suggest that NR may stimulate the cellular intake of nutrients including fatty acids and glucose in these renal cells, potentially increasing the storage, leading to lipid droplets accumulation.

NR supplementation increases renal mitochondrial content and modulates the SIRT3–SOD2 axis

Mitochondria play a central role in proximal tubular energy metabolism, and we expected that NR may protect from renal mitochondrial dysfunction induced by HFD. To investigate whether such effects are detectable in vivo, we assessed mitochondrial content in the renal cortex tissue using TOM20 immunostaining as a structural marker of the mitochondrial membrane. We observed a marked reduction in TOM20-positive staining in the kidneys of HFD-fed mice compared with LFD controls (P_diet < 0.0001), indicating a decrease in mitochondrial content under this condition of metabolic stress (Fig. 5a, b). In contrast, within the LFD groups, NR supplementation significantly increased TOM20 signal intensity (P_treatment < 0.001), consistent with an NR-mediated increased mitochondrial abundance (Fig. 5a, b). Moreover, Canto and colleagues demonstrated that NR supplementation induces SIRT3-dependent deacetylation of SOD2 in muscle tissue of obese mice[28]. To address whether SIRT3 was effectively activated in renal tissue by NR supplementation in LFD- and HFD-fed mice, we analyzed the abundance of acetylated SOD2 and lysine-acetylated proteins in the mitochondrial-enriched fraction of the renal cortex. HFD-fed mice display an increase in mitochondrial lysine-acetylated protein levels (P_diet < 0.05), but without an effect of NR treatment in our experimental conditions (Fig. 5c, d-h). However, a significant increase in the abundance of SOD2-acetylated form was observed in HFD-fed animals compared to LFD-fed ones (Fig. 5e). As expected, it suggests a decreased SIRT3 activity in mitochondria. Moreover, preventive and interventional NR treatment in HFD-fed mice significantly reduced the acetylation level of SOD2, confirming SIRT3 activation in response to NR in the renal tissue of obese mice. We also measured SIRT3 protein levels in mitochondrial-enriched renal cortex fractions (Fig. 5f). No significant difference was observed among groups. As previously reported, SIRT3 expression in HFD-fed animals does not always decline, whereas its activity can be impaired, as reflected by hyperacetylation of mitochondrial proteins[30,31].

NR supplementation protects human PTECs from PA-induced metabolic changes but not from LD accumulation

Given that NR supplementation only moderatly prevent renal dysfunction in vivo but increased lipid accumulation, we aimed to further investigate its effects at the cellular level. Specifically, we aimed to better characterize palmitic acid (PA)-induced lipotoxicity in PTECs and determine whether NR could exert protective effects by restoring NAD^+ levels or not. Using an in vitro model, we assessed whether NR could counteract PA-induced metabolic dysfunctions in human PTECs, independently of systemic factors. Different PA concentrations have been tested on HK-2 cells (human PTECs line) to trigger metabolic dysfunctions observed in obese mice. Therefore, HK-2 cells were treated from 100 to 700 µM of PA for 24 h (Supp. Figure 2). As observed, 300 µM of PA for 24 h led to a decreased NAD^+/NADH ratio and is associated with an increased positive staining of neutral lipids by Oil Red O and BODIPY 493/503 in HK-2 cells. Thus, regarding our data and previous studies, we decided to use a 300 µM concentration of PA for the following experiments. We next confirmed that a significant increase in NAD^+/NADH ratio was observed with 1 mM NR (Fig. 6a). Then, we wanted to determine whether NR-mediated restoration of the NAD^+/NADH ratio could protect HK-2 cells from deleterious consequences of PA-induced lipotoxicity. To address this question, HK-2 cells were exposed for 24 h to 0.4% BSA as a vehicle or 300 µM PA with or without 1 mM NR. NR significantly increases the NAD^+/NADH ratio in BSA- and PA-treated cells (Fig. 6b). NR treatment did not significantly affect the number nor the size of LD in PA-treated HK-2 cells (Fig. 6c-e), even if it significantly increased their metabolic activities assessed by MTT (3-[4,5-dimethylthiazol-2-yl]-2,5 diphenyl tetrazolium bromide) assay (Fig. 6f).

NR reduces PA-induced mitochondrial oxidative stress and lipid peroxidation in PTECs

ROS are short-lived oxygen-containing molecules known for their high reactivity, often promoting oxidative stress. These molecules are natural byproducts of aerobic respiration and primarily originate from mitochondria. PTECs are highly dependent on mitochondrial functions to sustain their metabolism, making them particularly vulnerable to mitochondrial damage[32]. PA, a saturated fatty acid, is well-documented for inducing oxidative stress, further exacerbating mitochondrial dysfunction in these metabolically demanding cells. As expected, PA treatment was associated with a significantly increased MitoSOX fluorescence indicative of mitochondrial ROS production when compared to BSA in HK-2 cells (Fig. 7a, b). This increased mitochondrial superoxide anion production was prevented upon NR supplementation in PA-treated cells. To confirm the benefits of NR on oxidative balance, its effect on lipid peroxidation was then addressed with a lipid peroxidation sensor that shifts from red to green in the presence of lipid hydroperoxides. The green-to-red fluorescence ratio was significantly increased in response to PA, indicating enhanced lipid peroxidation (Fig. 7a, c). This effect was

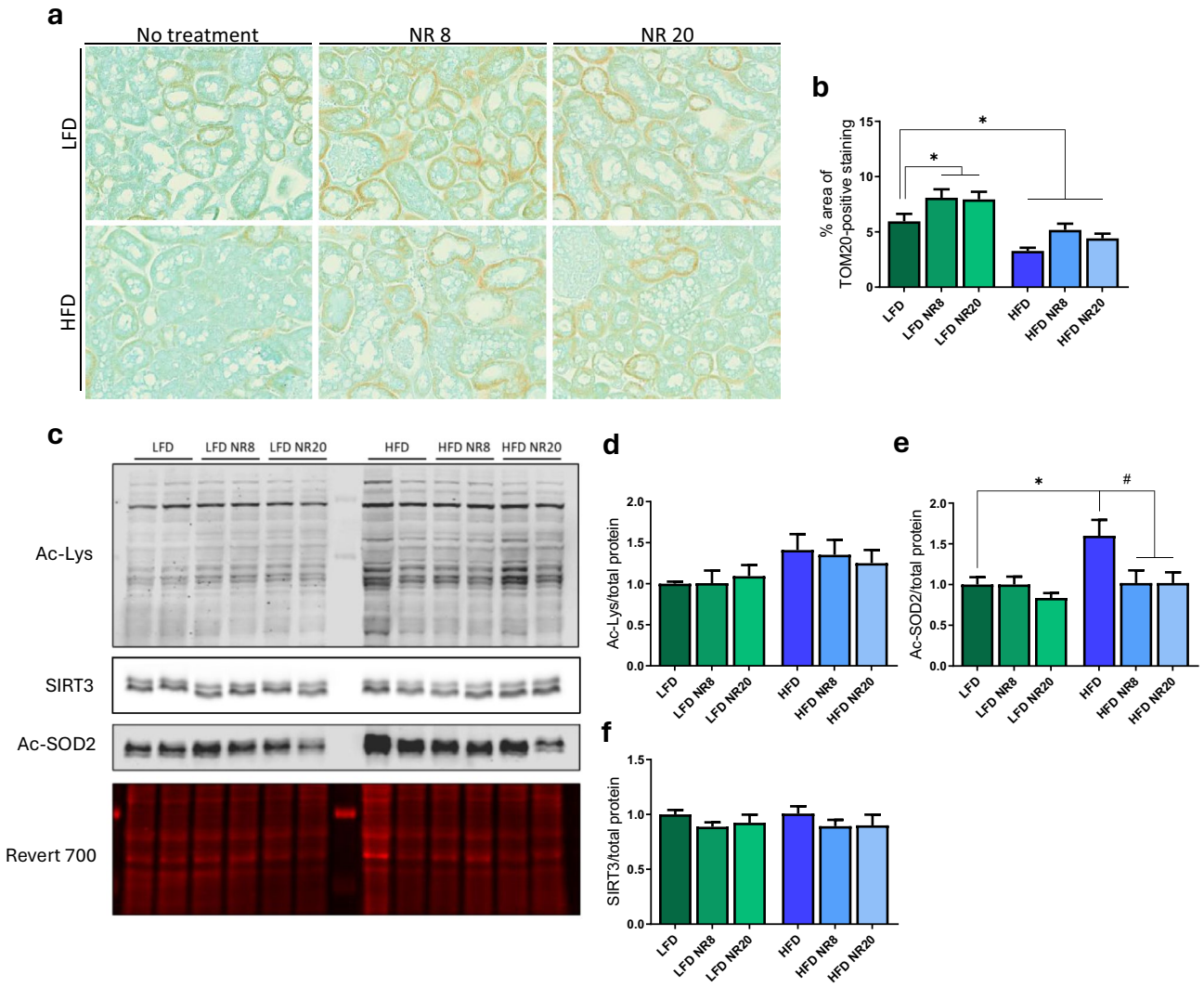

Fig. 5. NR supplementation increases renal mitochondrial content and modulates the SIRT3–SOD2 axis. **(a)** Representative photomicrograph (original magnification ×400) showing TOM20–positive staining on renal cortex section from LFD or HFD animals supplemented or not with NR at week 20. **(b)** Quantification of TOM20-positive area. For each mouse, 15 randomly selected fields were analyzed (6 mice per group; total of 90 fields per condition). Representative western blots and **(c-f)** quantitative densitometry analysis of acetylated lysine (Ac-Lys), acetylated SOD2 (Ac-SOD2, K68 residue), Sirtuin 3 (SIRT3) and total protein content (Revert 700) in mitochondria-enriched fractions from renal cortex of LFD or HFD animals supplemented or not with NR at week 20. Data is presented as means ± SEM, n = 4–6 in each group. Statistical analyses were performed by two-way ANOVA followed by Sidak's post hoc test. $^{*}p \leq 0.05$; $^{\#}p \leq 0.05$ between groups.

prevented by NR treatment. We further evaluated the abundance of SIRT3 and acetylated-SOD2 under these different experimental conditions (Fig. 7d-f). Consistent with our in vivo findings, acetylated form of SOD2 was less abundant in NR-treated cells when compared to the control group. Moreover, the abundance of SIRT3 was significantly reduced in PA-treated cells and significantly increased in cells exposed to NR treatment, when compared to cells incubated with PA alone. These findings confirm that NR induces SIRT3-mediated antioxidative response in PTECs.

NR prevents PA-induced mitochondrial damage in PTECs and regulates mitochondrial biogenesis and mitophagy

Given that NR induces an antioxidant response mediated by SOD2 and increases mitochondrial content in vivo, we hypothesized that it could modify the integrity of the mitochondrial network, protect mitochondrial activity, and support mitochondrial dynamics. We thus assessed the effects of NR on the morphology of the mitochondrial network in PA-treated cells. MitoTracker Green, a fluorescent probe that accumulates in mitochondria independently of their inner membrane potential, was used to visualise the mitochondrial network for each cell and to calculate the form factor, the ratio between endpoints to branched indicating network interconnectivity (Fig. 8a, b). BSA-treated cells displayed a filamentous and interconnected network while it appeared fragmented

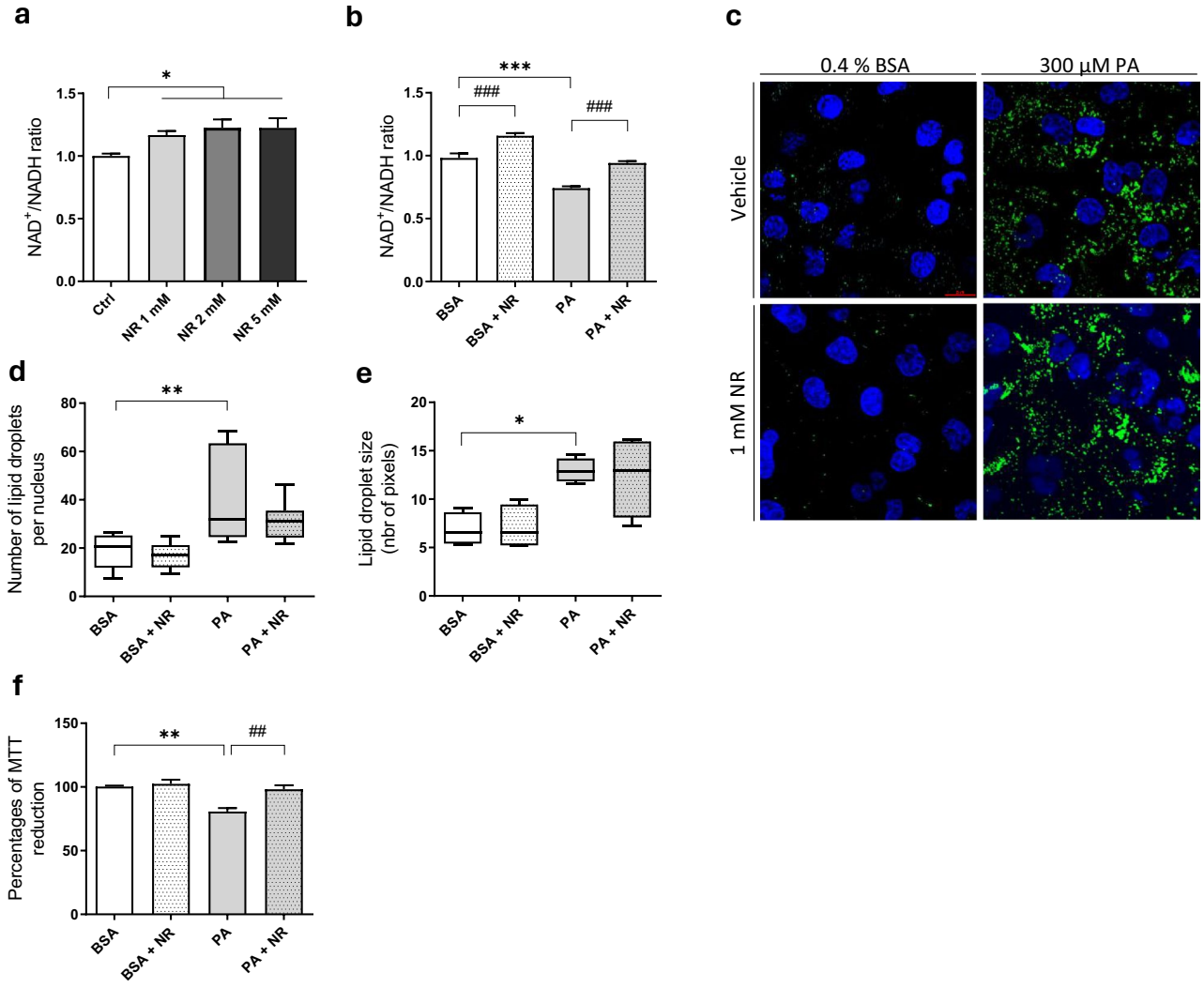

Fig. 6. NR treatment protects HK-2 cells from PA-induced metabolic changes but does not prevent lipid droplet formation. **(a)** Measurement of the NAD^+/NADH ratio using the NAD/NADH-Glo Assay Kit in HK-2 cells treated for 24 h with 1-, 2- or 5-mM NR or vehicle. **(b)** Measurement of the NAD^+/NADH ratio using the NAD/NADH-Glo Assay Kit in HK-2 cells treated for 24 h with 0.4% BSA or 300 µm PA with or without 1 mM NR. **(c)** Representative fluorescent photomicrographs of HK-2 cells treated for 24 h with 300 µM PA or 0.4% BSA with or without 1 mM NR and stained with 2.5 µM BODIPY™ 493/503 for 15 min (×400). **(d, e)** Quantifications of lipid droplet number and size on 100 cells per condition by Lipid Droplets MRI tool. **(f)** Percentages of MTT reduction (indicative of metabolic activities) in HK-2 cells treated for 24 h with 300 µM PA or 0.4% BSA with or without 1 mM NR. Data are presented as means ± SEM for experiments performed on whole-well averages, and as box plots (min to max) for single-cell image quantifications. All results are based on three independent biological experiments.. Statistical analyses were performed by **(a)** one-way ANOVA followed by Dunnett's post hoc test or by **(b, d, e, f)** two-way ANOVA followed Tukey's post hoc test. *$p \leq 0.05$; **$p \leq 0.01$; ***$p \leq 0.001$; $^{\#\#}p \leq 0.01$; $^{\#\#\#}p \leq 0.001$ between groups.

in PA-treated cells. This event was confirmed by a significantly increased form factor (mitochondrial endpoints to branched) in cells incubated with PA. Notably, PA-induced mitochondrial fragmentation was prevented by NR as the form factor was significantly reduced in cells treated with the combination of PA and NR when compared to PA alone. We next asked whether NR may be beneficial against PA-induced mitochondrial fragmentation by preventing an underlying event, mitochondrial depolarisation. HK-2 cells treated with BSA or PA with or without NR were thus stained with both the MitoTracker Red dye, which stains mitochondria with normal value of potential as well as the ratiometric JC-1 dye to assess depolarisation (Fig. 8c-d). PTECs treated with PA displayed a decrease in both MitoTracker Red fluorescence as well as JC1 590/510 ratio compared to control cells indicative of mitochondrial depolarisation, which was prevented by NR. Mitochondrial DNA (mtDNA) to nuclear DNA (nDNA) ratio was used to evaluate mitochondrial abundance. Surprisingly, mitochondrial content (mtDNA/nDNA) was decreased with NR supplementation, but the RNA expression of the mitochondrial transcription factor A (*TFAM*) and BCL2 Interacting Protein 3-like (*BNIP3L*) were increased in PA condition treated with NR

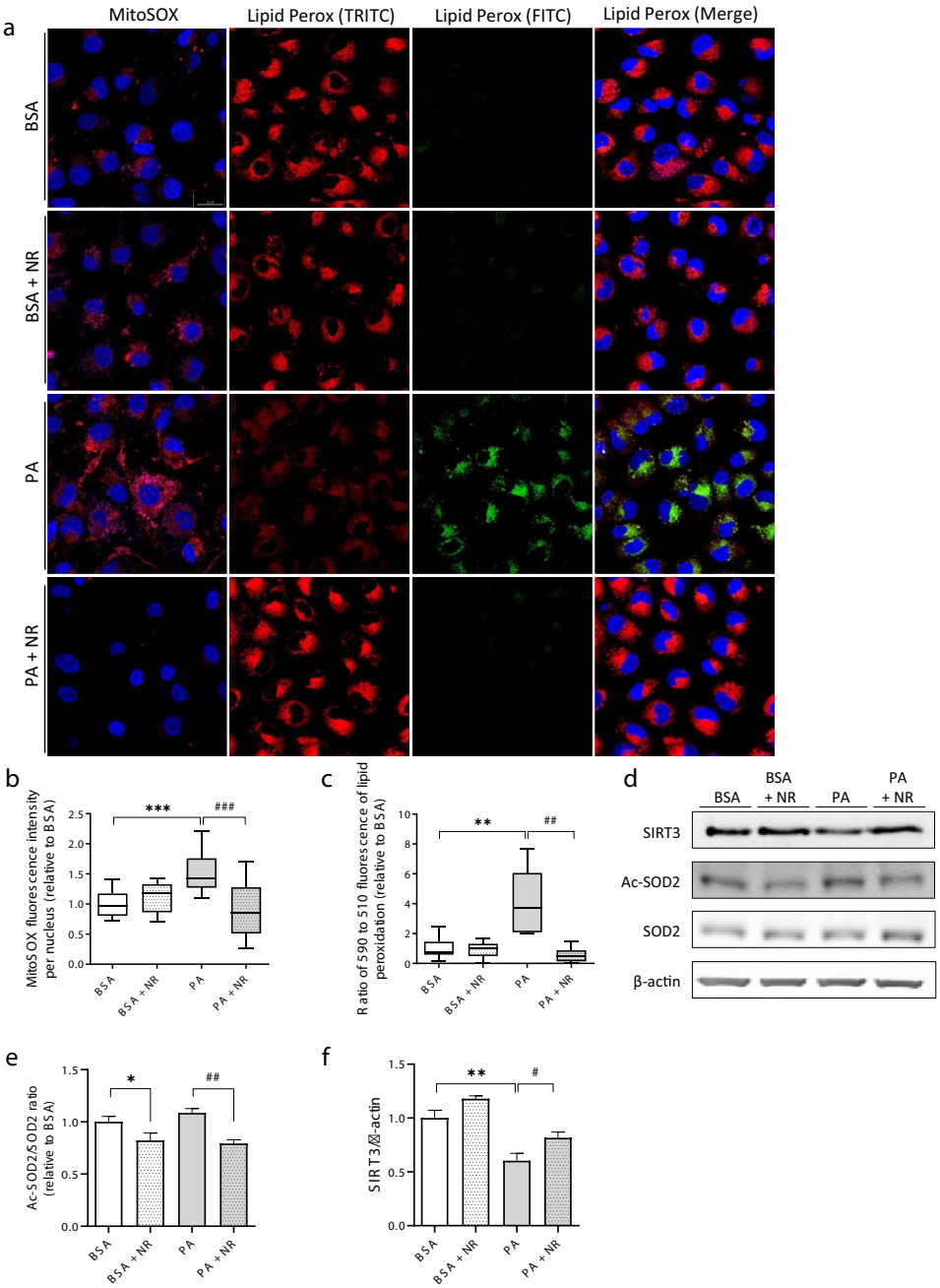

Fig. 7. NR treatment prevents PA-induced oxidative stress and lipid peroxidation in HK-2 cells. **(a)** Representative fluorescent photomicrographs of HK-2 cells treated for 24 h with 300 µM PA or 0.4% BSA with or without 1 mM NR and stained with 5 µM MitoSOX™ for 15 min (original magnification ×400) or with 10 nM Image-iT™ Lipid Peroxidation for 15 min (×400). **(b)** Quantification of the MitoSOX-relative fluorescence intensity per nucleus on more than 100 cells per experimental condition. **(c)** Quantitative analysis of the 590 to 510 nm ratio of fluorescence intensities linked to Image-iT™ Lipid Peroxidation staining on more than 100 cells per experimental condition. **(d)** Representative western blot and **(e, f)** quantitative densitometry analysis of SIRT3, acetylated SOD2 (Ac-SOD2, K68 residue), SOD2 and β-actin in HK-2 cells treated for 24 h with 300 µM PA or 0.4% BSA with or without 1 mM NR. Data are presented as means ± SEM for experiments performed on whole-well averages, and as box plots (min to max) for single-cell image quantifications. All results are based on three independent biological experiments. Statistical analyses were performed by two-way ANOVA followed Tukey's post hoc test. $^{*}p \le 0.05$; $^{**}p \le 0.01$; $^{***}p \le 0.001$; $^{\#}p \le 0.05$; $^{\#\#}p \le 0.01$; $^{\#\#\#}p \le 0.001$ between groups.

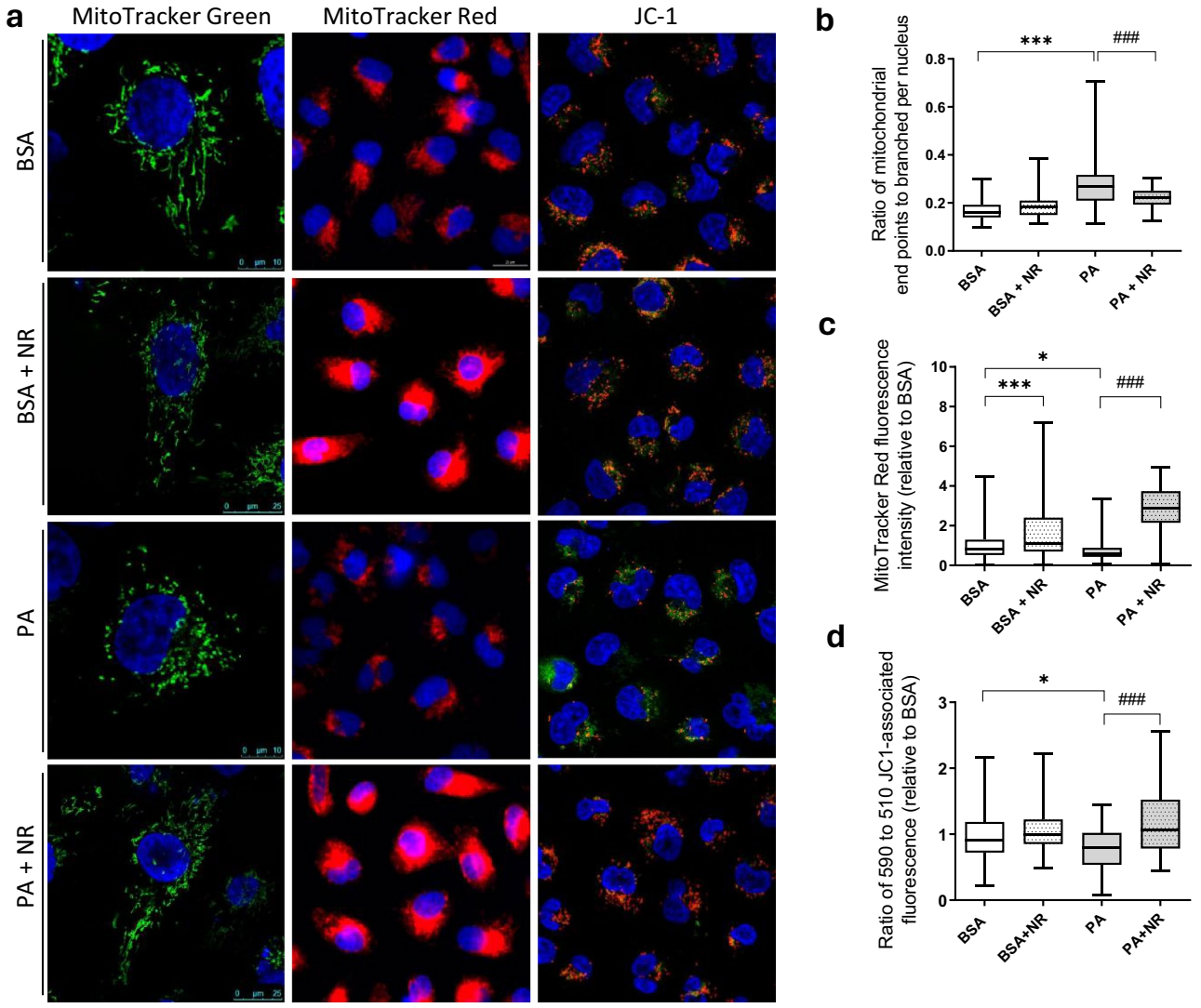

Fig. 8. NR treatment prevented PA-induced mitochondrial damage in HK-2 cells. **(a)** Representative fluorescent photomicrographs (original magnification ×600) of MitoTracker™ Green FM, MitoTracker™ Red CMXRos and MitoProbe™ JC-1 (original magnification ×400) probe staining in HK-2 treated with BSA 0.4%, PA 300 µM with or without NR 1 mM. Nuclei were counterstained with Hoechst Dye (blue). **(b)** Quantification of ratio between mitochondrial end points to branched on more than 100 cells per experimental condition. **(c)** Quantitative analysis of MitoTracker™ Red CMXRos fluorescence intensities on more than 100 cells per experimental condition. **(d)** Quantitative analysis of the 590 to 510 nm ratio of JC-1 fluorescence intensities on more than 100 cells per experimental condition. Data are presented as box plots (min to max). All results are based on three independent biological experiments. . Statistical analyses were performed by two-way ANOVA followed Tukey's post hoc test. $^{*}p \leq 0.05$; $^{***}p \leq 0.001$; $^{\#\#\#}p \leq 0.001$ between groups.

(Fig. 9a-c). Elevated *BNIP3L* expression indicates enhanced mitophagy, a biological process by which damaged or dysfunctional mitochondria are selectively degraded[33]. To functionally assess mitophagy regulation, we evaluated colocalization between lysosomes (LysoTracker staining) and mitochondria (MitoTracker staining) (Fig. 9d, e). Results suggested that PA reduced the colocalization of mitochondria with lysosomes after 24 h. NR treatment significantly increased the colocalization of mitochondria in lysosomes indicating enhanced mitophagy activity. These data confirm that NR functionally promotes mitophagy in tubular cells. This could explain the reduction in mtDNA/nDNA, as NR might promote the clearance of impaired mitochondria. Increased *TFAM* expression suggests that NR is promoting mitochondrial biogenesis. However, biogenesis may not yet fully compensate for the mitophagy-induced reduction in total mtDNA content, reflecting a dynamic mitochondrial turnover. Thus, our data suggests that NR could improve mitochondrial quality by balancing mitophagy and biogenesis, thereby promoting the replacement of damaged mitochondria.

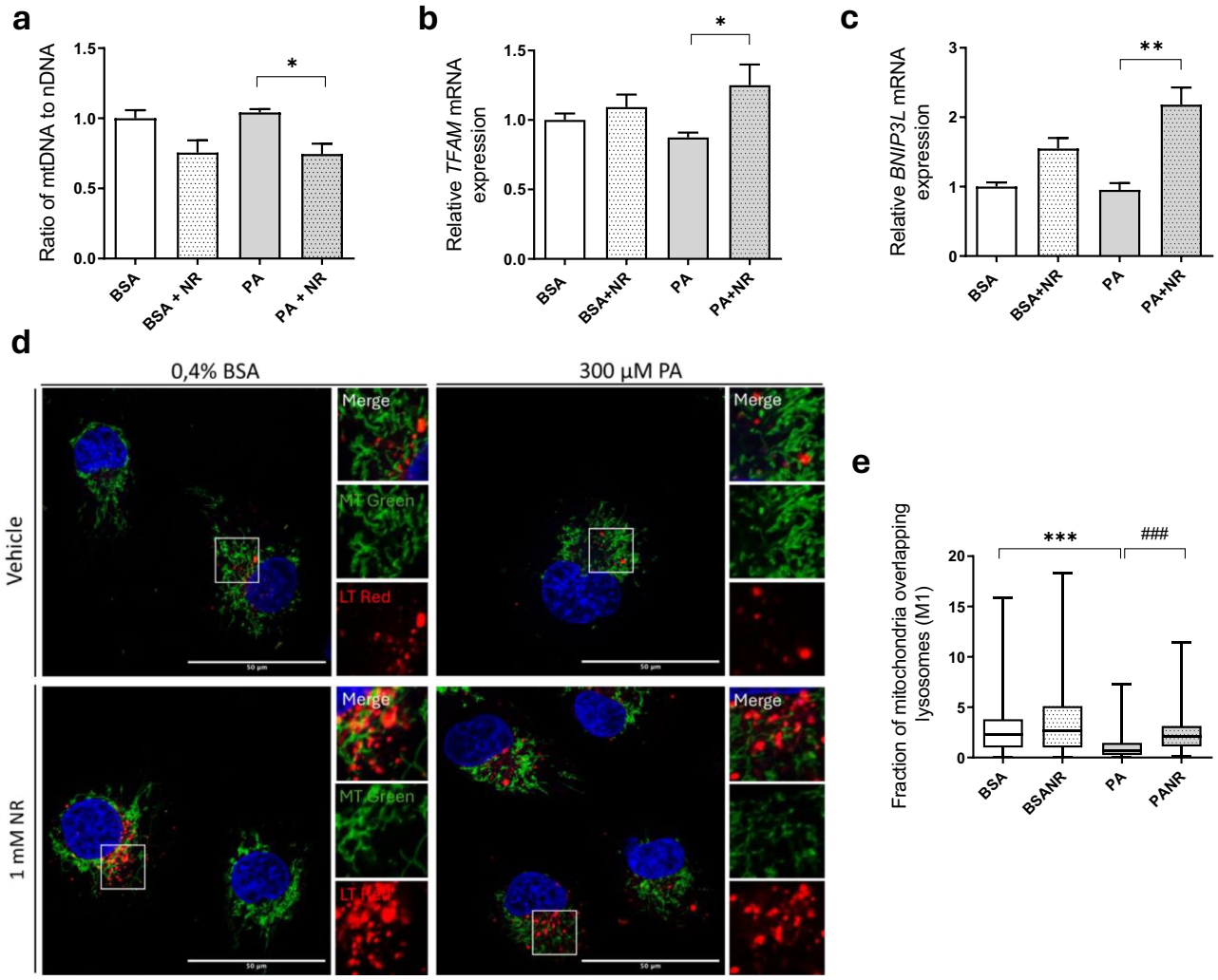

Fig. 9. NR regulates mitochondrial biogenesis and mitophagy in PA-treated HK-2 cells. **(a)** Quantitative analysis of the mitochondrial (mt) to nuclear (n) DNA ratio from HK-2 cells treated for 24 h with 300 µM PA or 0.4% BSA with or without 1 mM NR. **(b, c)** Relative mRNA expression of *TFAM* and *BNIP3L* in HK-2 cells treated for 24 h with 300 µM PA or 0.4% BSA with or without 1 mM NR. **(d)** Representative fluorescent photomicrographs of HK-2 cells treated for 24 h with 300 µM PA or 0.4% BSA with or without 1 mM NR and stained with MitoTracker™ Green and LysoTracker™ Red (original magnification ×600). **(e)** Mander's coefficient M1 of HK-2 exposed 24 h to PA 300 µM or BSA in combination or not with NR on more than 100 cells per experimental condition. Data are presented as box plots (min to max). All results are based on three independent biological experiments. Statistical analyses were performed by two-way ANOVA followed Tukey's post hoc test. *$p \leq 0.05$; **$p \leq 0.01$; ***$p \leq 0.001$; #$^{\#\#}p \leq 0.001$ between groups.

Discussion

Several studies have investigated the beneficial effects of NAD^+ precursors in mitigating diet-induced obesity[28,34,35]. However, to the best of our knowledge, no investigation has specifically explored the impact of NR supplementation on the kidneys in conditions of obesity and lipotoxicity. Both decreased NAD^+ biosynthesis pathway and NAD^+ consumption are responsible for NAD^+ reduction in AKI and DKD[36,37]. In AKI, endoplasmic reticulum stress response reduces de novo NAD^+ biosynthesis in the kidney by reducing QPRT expression[38]. Persistent QPRT reduction, a key enzyme of de novo NAD^+ biosynthesis, is associated with AKI to CKD progression. In DKD, reduced NAD^+ levels have been linked to decreased activity of the enzyme kynurenine 3-monooxygenase (KMO), also involved in the NAD^+ biosynthesis pathway[37]. Additionally, NAD^+-dependent enzymes, such as sirtuins and PARPs consume NAD^+ during DNA repair and stress responses, further contributing to NAD^+ depletion in both AKI and diabetes[16]. NAD^+ precursors such as Nicotinamide Mononucleotide (NMN) and NAM have been reported beneficial effects in renal injury by restoring NAD^+ levels, enhancing mitochondrial function, reducing oxidative stress and inflammation, preventing cellular senescence and fibrosis, and improving tubular cell function and survival[39–42]. In this study, we aimed to evaluate the effects of NR-mediated NAD^+ repletion in HFD-fed mouse model of CKD, previously established and characterized by our group[8,9,43]. NR has been found to be readily absorbed, to enhance NAD^+ levels more

effectively than other precursors, and to exhibit superior bioavailability as a form of vitamin B3 in both mice and humans[26]. Here, NR was used either as a preventive therapy (early administration of NR in the diet for 20 weeks) or as a treatment (delayed administration in the diet for the last 8 weeks of the protocol). Canto and colleagues demonstrated that 400 mg/kg/Day of NR treatment in HFD mice for 10 weeks increased plasma and intracellular NAD^+[28]. Here, we demonstrated that 400 mg/kg/Day of NR supplementation whether initiated early or late, was not associated with body weight loss or improvement of glucose intolerance, insulin resistance and inflammation. Several other studies have reported limited or no effect of NR supplementation on insulin sensitivity. Cartwright and colleagues demonstrated that while 8 weeks NR supplementation (500 mg/kg/day in drinking water) increased mitochondrial respiration in the muscle tissue, it did not counteract HFD-induced metabolic parameters, including glucose intolerance and hepatic lipid accumulation[44]. Moreover, in another study, NR supplementation (350 mg/kg/Day in the diet) for 14 weeks in mice fed a HFD since week 15 did not altered body weight or glucose tolerance but moderately improved insulin resistance[45]. Here, plasma cholesterol levels decreased following 20 weeks of NR supplementation in obese mice. However, this was not accompanied by a reduction in the liver steatosis score. More surprisingly, NR treatment in control mice was associated with an increased lipid deposition in the liver tissue without any sign of hepatic toxicity with NR. In contrast, NR was associated with beneficial effects regarding liver fibrosis as attested by collagen deposition that was markedly reduced in HFD mice supplemented with NR. Pham and colleagues reported the effects of NR supplementation for 20 weeks (400 mg/kg/Day in the diet) on hepatic fibrosis in mice fed a high-fat/high-sucrose/high-cholesterol diet[46]. Interestingly, they showed that NR reduced collagen accumulation in the liver but not lipid accumulation as we also observed in our study, suggesting that the protective effect of NR on liver fibrosis was independent of changes in liver steatosis. Next, we demonstrated for the very first time the ability of NR to activate SIRT3 in mitochondrial fraction of renal cortex as evidenced by the increased SIRT3-mediated deacetylation of SOD2. Although SIRT3 protein levels were unchanged across the experimental groups, this does not preclude functional modulation of SIRT3 activity through NR-dependent variations in NAD^+ availability, supported by the observed changes in mitochondrial protein acetylation. SIRT3 is a NAD^+-dependent deacetylase primarily localized to mitochondria, in which it regulates the activity of several metabolic and antioxidant enzymes through deacetylation. One of its well-established substrates is SOD2, a mitochondrial enzyme critical for detoxifying ROS[47]. The deacetylation of SOD2 by SIRT3 enhances its enzymatic activity, contributing to improved mitochondrial oxidative defense. Reduced SIRT3 activity and SOD2 hyperacetylation thus contribute to oxidative stress and associated mitochondrial dysfunction[18]. HFD consumption has been shown to increase SOD2 acetylation[48]. Canto and colleagues have demonstrated that NR induces SIRT3-mediated SOD2 deacetylation in the skeletal muscle, liver, and brown adipose tissue but not in brain and white adipose tissue[28]. In our experimental model, HFD mice exhibited increased acetylation of mitochondrial SOD2 in renal tissue, that was completely reversed by NR supplementation. Our in vivo assessment based on TOM20 immunostaining also supports an effect of NR on mitochondrial content. However, the absence of functional and mitophagy-specific measurements remains a limitation. Other preclinical studies reported that NR enhances mitochondrial NAD^+ concentrations and activates mitochondrial biogenesis pathways in vivo, resulting in increased mitochondrial content in muscle and liver tissues[28]. Although incomplete, these findings are in line with the in vitro data showing mitochondrial homeostasis regulation by NR. Nevertheless, it is important to note that in the in vivo model, NR is delivered through the diet, leading to a mode of bioassimilation that differs from in vitro conditions in which NR is applied directly to the cells. We also evaluated the effects of NR on kidney function, glomerular and tubular injuries. The results indicate that NR supplementation in HFD mice has a limited impact on obesity-induced kidney injury. Specifically, NR induced only a moderate reduction in albuminuria, observed exclusively in the HFD group supplemented with NR for the last 8 weeks of the protocol. However, it did not significantly alter glomerular hypertrophy. Additionally, NR supplementation did not significantly reduce ectopic lipid accumulation in tubular cells, consistent with findings in the liver. Our data suggests that NR may enhance nutrient uptake through upregulation of CD36 and SGLT2 in PTECs, but the precise mechanisms driving the unexpected renal and hepatic lipid accumulation under physiological conditions remain to be fully investigated. Moreover, we further characterized the effects of NR on human PTECs (HK-2 cells). Cells were exposed to PA to mimic obesity in vitro. PA is the most abundant saturated FA in the western diet[49]. Exposition with PA is widely used to investigate lipotoxicity on renal cell cultures[50–52]. Here, NR treatment was associated with NAD^+ repletion and an improvement in metabolic activity in PTECs exposed to PA. However, this was not accompanied by a reduction in intracellular LD, similarly to what is observed in the renal tissue of obese mice treated with NR. Moreover, the acetylation level of SOD2 was found to be decreased in response to NR, likely mediated by the activation of SIRT3. NR treatment was also associated with a reduction in mitochondrial ROS and the subsequent lipid peroxidation triggered by PA exposure. NR also counteracted the detrimental effects of PA on mitochondrial structure and integrity. This indicates that NR supports mitochondrial health and functionality, which are compromised under lipotoxic conditions. These improvements may underline the broader protective effects of NR against cellular oxidative stress and metabolic dysfunction in this context. Specifically, NR treatment alleviates the alterations in the mitochondrial network induced by PA. Moreover, NR reduces mitochondrial content in PTECs, most likely not through decreased mitochondrial biogenesis but rather by an increased mitochondrial degradation as evidenced by the upregulation of the mitophagy receptor BNIP3L. This observation is supported by a study showing that enhancing NAD^+ levels with precursors promotes mitophagy, thereby maintaining mitochondrial homeostasis[53]. In another study, NR supplementation was also shown to elevate NAD^+ levels, which in turn increased the expression of BNIP3L in human neurons derived from Parkinson's disease patients[54]. Lastly, a study found that increasing NAD^+ levels via NR supplementation restored mitophagy in a *C. elegans* model of accelerated aging through the worm homolog of BNIP3L[55]. This upregulation of BNIP3L could facilitate the clearance of damaged mitochondria through mitophagy, thereby ameliorating mitochondrial dysfunction associated with the disease. Our study has several limitations. The

absence of TEM-based ultrastructural analyses in the current study limits the direct assessment of mitochondrial morphology, mitophagy, and lysosomal alterations, which would have further strengthened the mechanistic interpretation. Moreover, although the vacuolar structures observed in the present study are consistent with previously characterized phospholipid-rich lysosomal inclusions, the lack of complementary lipid-specific analyses represents a limitation for definitively confirming their nature. Next, the lack of mechanistic and long-term functional investigations represents a limitation for fully interpreting the unexpected NR-induced lipid accumulation observed in kidney and liver under control dietary conditions. Although this study primarily focused on the direct renal effects of NR, it is important to consider potential systemic influences, particularly through the liver–kidney axis. NR has been shown to improve hepatic function, which may indirectly affect renal physiology by modulating circulating metabolites and inflammatory pathways[56]. Here, we did observe mild changes in hepatic parameters, particularly increased hepatic steatosis but decreased fibrosis while liver dysfunction in HFD-fed mice was not improved with NR treatment. These potential systemic effects represent a limitation of our current study and warrant further investigation using tissue-specific approaches. Lastly, NR responsiveness is tissue-dependent, as shown by others[57], and that subcellular NAD^+ compartmentalization[58] in renal cells in vivo may contribute to the modest renal or mitochondrial effects observed in our study despite measurable molecular responses.

Conclusion

Our study, in line with others, demonstrates that NR supplementation is well-tolerated but offers moderate beneficial effects on obesity-related conditions. However, its efficacy may vary depending on factors such as dose, treatment duration, animal source, administration method, and sex. Notably, emerging evidence indicates that high doses or prolonged NR treatment may cause adverse effects such as glucose intolerance and white adipose tissue dysfunction due to decreased metabolic flexibility in mice[59,60]. Under our experimental conditions, NR yielded minimal improvements in metabolic parameters. It induced fat deposition in the kidney and liver in control animals, with more pronounced effects over extended treatment durations. Importantly, NR had no negative impact on kidney or liver function and moderately ameliorated obesity-induced renal impairments, including reductions in albuminuria and oxidative stress. In PTECs, NR enhanced mitochondrial dynamics, mitophagy and triggered a robust antioxidant response, likely linked to SIRT3 activation, although it did not reduce lipid accumulation. Given ongoing clinical trials, further research is crucial to refine administration strategies and better understand potential adverse effects associated with NAD^+ precursors.

Material and methods

Animals

The study conformed to the APS Guidelines for the Care and Use of Animals and was approved by the Animal Ethics Committee of the University of Namur. The study was conducted in accordance with ARRIVE guidelines. The experiments were conducted on C57Bl/6 J male mice (Janvier Labs, Le Genest Saint-Isle, France) that were housed in cages with free access to food and water. Mice were maintained at 35–40% relative humidity and a temperature of 20–23 °C with a 12:12 h light–dark cycle. Eight-weeks old mice were randomized to either a low-fat diet (LFD, 10% of total calories from fat; D12450J, Research Diets, New Brunswick, NJ, USA) or a high-fat diet (HFD, 60% of total calories from fat; D12492, Research Diets, New Brunswick, NJ, USA) supplemented or not with 400 mg/kg/Day of Nicotinamide Riboside (NR; Niagen, ChromaDex, Irvine, CA; prepared by Research Diets; D19052102 and D19052103) from week 0 or week 12 for a total of 20 weeks period. After 20 weeks, mice were euthanized after an overnight fast with a solution of ketamine (Nimatek®, Eurovet Animal Health, Blabel, The Netherlands, 80 mg/kg b.w.) and medetomidine (Domitor®, Orion Pharma, Espoo, Finland, 0.5 mg/kg b.w.), blood was collected by intracardiac puncture while kidneys were dissected into cortex and medulla. A kidney portion of cortex was freshly processed for mitochondrial isolation with the Mitochondria Isolation Kit for Tissue (Thermo Fisher Scientific, Waltham, MA, USA), following manufacturer's instructions. Then, each renal sample was snap-frozen in liquid nitrogen for further analysis. An additional portion was fixed in 4% paraformaldehyde (PAF) for histological analysis. Mice were placed in metabolic cages for 24-h urine collection at baseline and at the end of the protocol. Urinary albumin and creatinine levels were measured using a mouse Albuwell ELISA kit and Creatinine Companion kit (Exocell, Philadelphia, PA, USA).

Glucose tolerance test

After a 12 h-overnight fast, a GTT was performed at weeks 0, 12 and 20 of the experimental protocol. A dose of 2 g/kg body weight of D-glucose (Roth, Karlsruhe, Germany) was administered intraperitoneally. Blood samples were then obtained from the caudal vein, and the blood glucose level was measured at 0, 30, 60, and 120 min after glucose injection using a One Touch® Verio glucometer (Zug, Switzerland).

Biochemical assays

Plasma insulin levels were determined by ELISA using the rat/mouse insulin ELISA kit (Merck, Darmstadt, Germany). The homeostasis model assessment (HOMA-IR) for the insulin resistance index was determined using a calculator available from the Oxford Center for Diabetes, Endocrinology, and Metabolism (https://www.dtu.ox.ac.uk/homacalculator/). Plasma IL-6 concentration was measured according to the manufacturer's instructions (Mouse Interleukin-6 (IL-6) ELISA Kit; Gentaur, Kampenhout, Belgium). Colorimetric enzymatic test was performed to measure plasma cholesterol levels (Diasys, Diagnostic System, Holzheim, Germany) following the manufacturer's instructions. Plasma concentrations of urea nitrogen (Abcam, Cambridge, United Kingdom, ab83362), Cystatin-C (R&D Systems, Minneapolis, USA, MMSCTC0) and creatinine (Crystal Chem, Elk Grove Village, USA, 80350) were also evaluated following the manufacturer's instructions. Plasma hepatic

biomarkers (GOT and GPT) were investigated using Spotchem EZ SP-4430 analyzer and the Spotchem II Liver-1 kit (Arkray, Amstelveen, Netherlands, 77182).

Histology and morphological analyses

Five-µm paraffin-embedded kidney sections were stained with Periodic Acid Schiff (PAS), Hemalun, and Luxol Fast Blue to assess morphological alterations. Morphometry of kidney sections was performed as previously reported[7]. Briefly, the percentage of tubules containing vacuolated cells was evaluated using a semi-quantitative single-blind analysis. Paraffin-embedded liver sections were stained with hematoxylin and eosin and steatosis was graded as described by Ryu and colleagues[61]. To evaluate fibrosis, paraffin-embedded liver and kidney sections were stained with picrosirius red (collagen I and III deposits). To standardize the evaluation procedure, an additional lens engraved with a square grid was inserted into one of the microscope eyepieces. For each paraffin section, 10 square fields (0.084 mm^2/field) were observed at ×400 magnification. Ten randomly selected areas of each cortex kidney or liver section were analyzed using the ImageJ software.

Immunohistochemistry

Five-µm paraffin-embedded kidney sections were dewaxed and rehydrated. Renal tissue antigens were unmasked using microwave pretreatment in SignalStain® Citrate Unmasking Solution (Cell Signaling, Danvers, MA, USA, 14746). Endogenous peroxidase activity was inhibited by incubation with 3% H_2O_2 for 10 min and subsequently blocked with Animal-Free Blocking Solution (Cell Signaling, Danvers, MA, USA, 15019). The primary antibody against TOM20 (Abcam, Cambridge, United Kingdom, ab186734) was incubated overnight at 4 °C. After rinsing in TBS-Tween, slides were exposed for 30 min to SignalStain® Boost IHC Detection Reagent (Cell Signaling, Danvers, MA, USA, 8114) and bound peroxidase activity was detected using a DAB kit (Cell Signaling, Danvers, MA, USA, 8059). Counterstaining was performed with hemalum and Luxol Fast Blue. For each renal cortex section, 10 square fields (0.084 mm^2 per field) were examined at ×400 magnification. Randomly selected areas from each kidney cortex section were analyzed using ImageJ software. The proportion of the area showing positive staining was quantified and expressed as a percentage.

Western blot analysis

Proteins from mitochondrial-enriched renal cortex sample or HK-2 cells were extracted using Cell Lysis Buffer (Cell Signaling, Danvers, MA, USA) with phosphatase and protease inhibitor cocktail (Thermo Fisher Scientific, Waltham, MA, USA) at 4 °C followed by centrifugation at 14,000 × g for 15 min at 4 °C. Protein concentrations were quantified by Pierce BCA assay kit (Thermo Fisher Scientific, Waltham, MA, USA) and 20 µg of total lysate were separated by SDS-PAGE 12% and transferred onto nitrocellulose membranes. Membranes were stained with Revert™ 700 Total Protein Stain (Li-Cor Biosciences, Lincoln, NE, USA). Following blocking step in 5% BSA for 1 h, the membranes were incubated with primary antibodies against SIRT3 (Cell Signaling), acetyl K68-SOD2 (Abcam), SOD2 (Abcam), pan-acetyl lysines (Abcam) or β-actin (Thermo Fisher Scientific, Waltham, MA, USA) overnight at 4 °C and then with secondary antibodies (Li-Cor Biosciences, Lincoln, NE, USA) for 1 h at room temperature. Antibodies were diluted in Odyssey Blocking Buffer TBS containing 0.1% Tween 20. Proteins were visualized and quantified using the Odyssey® imaging system (Li-Cor Biosciences, USA).

Cell culture and treatments

HK-2 cells (Human Kidney 2, ATCC® CRL-2190™, Belgium) were cultivated in DMEM/F12 (Thermo Fisher Scientific, Waltham, MA, USA) supplemented with 10% fetal bovine serum (FBS, Gibco), 1000 U/L penicillin, 100 µg/mL streptomycin in an atmosphere containing 5% CO_2 at 37 °C. Sodium palmitate (Sigma-Aldrich, P9767) was added in 10% free-fatty acid (FA) BSA (Sigma-Aldrich, A8806) solution at 37 °C under agitation to reach PA concentration of 7.5 mM stock solution and a PA/BSA molar ratio of 5:2. The concentration was assessed after each complexation using the non-esterified FA assay kit (Fujifilm WAKO, 434–91795 and 436–91995,). HK-2 cells were treated with 300 µM PA or BSA as a vehicle with or without 1 mM Nicotinamide Riboside (NR) (Niagen, ChromaDex, Irvine, CA) for 24 h.

Viability assay

Cell viability was assessed indirectly by staining with crystal violet dye, as described by Journe and colleagues[62]. Briefly, HK-2 were seeded in 96-well plates at a density of 10.000 cells/well in complete DMEM/F12 medium for 18 h. After 24 h treatment, cells were gently rinsed with phosphate-buffered saline (PBS), fixed with 1% glutaraldehyde (Sigma-Aldrich, G7776)/PBS for 15 min and stained with 0.1% crystal violet (Sigma-Aldrich, HT901; weight/vol in double distilled H_2O) for 30 min. Cells were washed under running tap water for 15 min and subsequently lysed with 0.2% Triton X-100 (vol/vol in double distilled H_2O). The absorbance was measured at 550 nm in a spectrophotometer (SpectraMax ID5, Molecular Devices, USA).

Metabolic activity

Metabolic activity of cells was assessed by MTT colorimetric assay (Promega, Madison, WI, USA). HK-2 cells were seeded on a 96-well plate at a density of 10.000 cells/well in complete DMEM/F12 medium for 18 h and then treated with BSA/PA during 24 h. Cells were then incubated with MTT (50 µg/well) for 2 h. The supernatant was removed and 100 µl dimethylsulfoxide was subsequently added to each well. After shaking the plate, the absorbance of each well was measured at 570 nm in a spectrophotometer (SpectraMax ID5, Molecular Devices, USA).

Measurement of lipid droplets content

LD were observed using BODIPY 493/503 fluorescent lipid probe (Thermo Fisher Scientific, Waltham, MA, USA, D3922). 50.000 cells/well were seeded in 2-well Nunc Lab-Tek Chamber Slide System (Thermo Fisher Scientific, Waltham, MA, USA) for 18 h. After 24 h treatment, cells were washed 3 times with PBS and incubated with 1 mL/well of DMEM/F12 containing 2.5 µM of BODIPY 493/503 and 3.75 µg/mL of Hoechst 33342 (Miltenyi Biotec, Germany) for 15 min at 37 °C. Then, cells were washed 3 times with PBS and immediately examined under a confocal microscope (Leica Microsystems). Quantifications of LD size and number were performed using FIJI v.2.1.0. and the "*MRI Lipid Droplets Tool*" plugin. Quantification was performed on five randomly selected photomicrographs per condition, with each containing 25 cells. For Oil Red O staining, cells were first rinsed three times with 1X PBS and then fixed with 4% PFA for 30 min at room temperature. After fixation, the cells were rinsed three times with PBS, followed by a single rinse with 60% isopropanol. They were then left to dry at room temperature for 10 min until the liquid had fully evaporated. The Oil Red O staining solution (Sigma-Aldrich, Saint-Louis, MO, USA) was added, and cells were incubated with the stain for 2 h at room temperature. After incubation, cells were rinsed four times with PBS. Finally, coverslips with the cultured cells were mounted onto slides using ImmunoHistoMount™ mounting medium (Sigma-Aldrich, Saint-Louis, MO, USA).

NAD^+/NADH ratio assessment

NAD^+ levels were measured using the NAD/NADH-Glo Assay Kit (Promega, Madison, WI, USA) following manufacturer's instructions. Briefly, cells were seeded on 24-well plate at a density of 50.000 cells/well in complete DMEM/F12 medium for 18 h. Cells were then exposed to treatments for 24 h as described before. Cells were washed in PBS and lysed with 220 µL/well of 1% dodecyltrimethylammonium bromide solution. The content of each well was divided in two to measure NAD^+ and NADH separately. To measure NAD^+, 50 µL of 0.4 N HCl were added, and cell lysates were heated at 60 °C for 15 min. Samples were incubated at room temperature for 10 min and 50 µL of Trizma base® were added. To measure NADH, cell lysates were heated at 60 °C for 15 min, incubated at room temperature for 10 min and 50 µL of HCl/Trizma® solution were added. Finally, 25 µL of cell lysates were loaded in an opaque 96-well plate as well as 25 µL of the NAD + /NADH-Glo™ Detection Reagent containing Ultra-Glo™ Luciferase, Reductase, Reductase Substrate, NAD^+ Cycling Enzyme and NAD^+ Cycling Susbtrate. After an incubation of 30 min at room temperature, luminescence was recorded using a spectrophotometer (SpectraMax ID5, Molecular Devices, USA).

Staining of the mitochondrial network

The mitochondrial network was stained through different probes; MitoTracker™ Red CMXRos (Thermo Fisher Scientific, Waltham, MA, USA, M7512), whose accumulation is dependent upon membrane potential and MitoTracker™ Green FM (Thermo Fisher Scientific, Waltham, MA, USA, M7514) whose accumulation is not. In addition, the MitoProbe™ JC-1 (Thermo Fisher Scientific, Waltham, MA, USA, M34152) was used and allowed detection of changes in mitochondrial membrane potential indicated by fluorescence emission shift from green to red. Briefly, 50.000 cells/well were seeded in 2-well Nunc Lab-Tek Chamber Slide System for 18 h. After a 24 h-treatment, cells were incubated for 30 min at 37 °C with 1 mL/well of DMEM/F12 containing 3.75 µg/mL of Hoechst and 50 nM of MitoTracker™ Red or Green or 200 µM of JC-1. Then, cells were rinsed 3 times with PBS and immediately examined under a confocal microscope (Leica Microsystems). Mitochondrial network morphology analysis was performed based on MitoTracker™ Green staining. The form factor which is the ratio between end and branched points was calculated with the ImageJ software on 30 randomly selected photomicrographs containing individual cell per condition. The intensity of fluorescence of MitoTracker™ Red and the JC-1 related fluorescence shift from 590 to 510 nm were calculated using the ImageJ software on five randomly selected photomicrographs containing 25 cells per condition.

Assessment of mitochondrial and cytosolic oxidative stress

Mitochondrial superoxide generation was detected using MitoSOX™ Red Mitochondrial Superoxide Indicator (Thermo Fisher Scientific, Waltham, MA, USA, M36008). This dye selectively targets mitochondria, where it is oxidized by superoxide anion radicals, resulting in red fluorescence. In parallel, lipid peroxidation was assessed by the Image-iT™ Lipid Peroxidation (Thermo Fisher Scientific, Waltham, MA, USA, C10445) which shifts from red to green upon oxidation and thus provides a ratio metric indication of lipid peroxidation.

For both stainings, 50.000 cells/well were seeded in 2-well Nunc Lab-Tek Chamber Slide System for 18 h. After 24 h treatment, cells were incubated for 15 min at 37 °C with 1 mL/well of DMEM/F12 containing 3.75 µg/mL of Hoechst and 5 µM MitoSOX or 10 nM lipid peroxidation dye. Then, cells were washed 3 times with PBS and immediately examined under a confocal microscope (Leica Microsystems). MitoSOX-related mean fluorescence intensity and the fluorescence shift from 590 to 510 related to lipid peroxidation were obtained through ImageJ from five randomly selected fields per condition, with each containing 25 cells.

Assessment of the colocalization of mitochondria and lysosomes

Mitochondria were labeled using MitoTracker™ Green probe (Thermo Fisher Scientific, Waltham, MA, USA, M7514). This neutral and lipophilic dye accumulates within mitochondria independently of the mitochondrial membrane potential, thereby detecting all mitochondria and resulting in green fluorescence. In parallel, lysosomes were labeled using LysoTracker™ Red DND-99 (Thermo Fisher Scientific, Waltham, MA, USA, L7528), which emits red fluorescence once protonated in acidic cellular compartment such as lysosomes. Cells were seeded at a density of 20.000 cells/well in 35 mm high µ-Dishes (Ibidi, Gräfelfing, Germany, 81156) for 24 h. After 24 h treatment, cells were incubated for 30 min at 37 °C with 1 mL/well of HBSS containing 3.75 µg/mL of Hoechst, 500 nM of MitoTracker Green, and 30 nM of LysoTracker Red. Cells were then washed 3

Gene		Primer sequences (5'-3')
TFAM	Fw	GTGGGAGCTTCTCACTCTGG
	Rv	TAGGGCTTTTTCTCCTGCAA
BNIP3L	Fw	TTGGATGCACAACATGAATCAGG
	Rv	TCTTCTGACTGAGAGCTATGGTC
ND1	Fw	ACACTAGCAGAGACCAACCG
	Rv	GAAGAATAGGGCGAAGGGGC
ACTB	Fw	TCACCCACACTGTGCCCATCTACGA
	Rv	CAGCGGAACCGCTCATTGCCAATGG
18S (human)	Fw	TGGTGCATGGCCGTTCT
	Rv	TAGTTAGCATGCCAGAGTCTCGTT
Cd36	Fw	TGCATTTGCCAATGTCTAGC
	Rv	CCTTAAAGGAATCCCCGTGT
Slc5a2	Fw	CATGTCCACTGAGATCTTGGTGAA
	Rv	CCGCATCCGCCTCTACCT
18S (mouse)	Fw	CGCCGCTAGAGGTGAAATTCT
	Rv	CGAACCTCCGACTTTCGTTCT

Table 1. Primer sequences for RT-qPCR analysis of mRNA expression.

times with PBS and incubated in HBSS before immediate examination under a confocal microscope (Leica Microsystems). Fifteen photomicrographs, each containing one to four cells, were acquired by condition using a ×600 magnification. Image analysis was performed in ImageJ using the JaCoP (Just Another Colocalization Plugin) plugin to calculate Mander's coefficients M1.

DNA or RNA extraction and RT-qPCR

Total DNA extraction from HK-2 cells was performed using the QIAamp DNA Mini Kit (Qiagen, 51304). Following this extraction, an RNase A treatment (Sigma Aldrich, 11119915001) is carried out to degrade any present RNA. Total DNA concentration was measured using NanoDrop 1000 (Thermo Fisher Scientific, Waltham, MA, USA). Total RNA from HK-2 cells was extracted with Trizol (Sigma-Aldrich) and treated with DNAse (Promega). Then, total RNA concentration was measured using NanoDrop 1000 (Thermo Fisher Scientific, Waltham, MA, USA). Reverse transcription was performed with the Transcriptor First Strand cDNA Synthesis Kit (Roche Applied Science, 04897030001) to convert 1 µg of RNA into cDNA. The NCBI Primer BLAST was used to ensure the specificity of the primers for each target. All primer pairs were analyzed for their dissociation curves and melting temperatures. Real-time quantitative PCR was performed to quantify the mRNA levels of *Tfam, Bnip3l, Nd1, Actb* and *18S* as housekeeping gene (Table 1). Quantitative PCR amplification was performed using SYBR Green Master Mix (Roche, Belgium) and Prism 7300 Real-Time PCR Detection System (Applied Biosystems, CA, USA). Mean fold changes were calculated by averaging triplicate measurements for each gene. The relative gene expression was calculated using the $2^{-\Delta\Delta CT}$ method.

Statistical analysis

Results are presented as mean values ± SEM. The level for statistical significance was defined as $p < 0.05$. Analyses were carried out using Prism GraphPad Software version 8. Differences between data groups were evaluated using one- or two-way ANOVA followed by Sidak's, Dunnett's or Tukey's post hoc tests for multiple comparisons. The level of significance was defined as 0.05 and p values were indicated by symbols in the Figure legends. All biological-independent experiments were performed at least three times or more as indicated in the legends of the figures.

Data availability

The datasets generated during and/or analyzed during the current study are available from the corresponding author on reasonable request.

Received: 5 June 2025; Accepted: 24 March 2026
Published online: 09 April 2026

References

1. González-Muniesa, P. et al. Obesity. *Nat. Rev. Dis. Primers.* **3**, 17034 (2017).
2. Han, T. S. & Lean, M. E. A clinical perspective of obesity, metabolic syndrome and cardiovascular disease. *JRSM Cardiovasc. Dis.* **5**, 2048004016633371 (2016).
3. Garofalo, C. et al. A systematic review and meta-analysis suggests obesity predicts onset of chronic kidney disease in the general population. *Kidney Int.* **91**, 1224–1235 (2017).
4. D'Agati, V. D. et al. Obesity-related glomerulopathy: clinical and pathologic characteristics and pathogenesis. *Nat. Rev. Nephrol.* **12**, 453–471 (2016).
5. de Vries, A. P. J. et al. Fatty kidney: Emerging role of ectopic lipid in obesity-related renal disease. *Lancet. Diabetes. Endocrinol.* **2**, 417–426 (2014).

6. Yamamoto, T. et al. High-fat diet-induced lysosomal dysfunction and impaired autophagic flux contribute to lipotoxicity in the kidney. *J. Am. Soc. Nephrol. JASN* **28**, 1534–1551 (2017).
7. Declèves, A.-E. et al. Regulation of lipid accumulation by AMK-activated kinase in high fat diet–induced kidney injury. *Kidney Int.* **85**, 611–623 (2014).
8. Juszczak, F. et al. Delayed exercise training improves obesity-induced chronic kidney disease by activating AMPK pathway in high-fat diet-fed mice. *Int. J. Mol. Sci.* **22**, 350 (2020).
9. Juszczak, F. et al. Sex differences in obesity-induced renal lipid accumulation revealed by lipidomics: a role of adiponectin/AMPK axis. *Biol. Sex Differ.* **14**, 63 (2023).
10. Sun, Y. et al. High-fat diet promotes renal injury by inducing oxidative stress and mitochondrial dysfunction. *Cell. Death. Dis.* **11**, 1–14 (2020).
11. Forbes, J. M. & Thorburn, D. R. Mitochondrial dysfunction in diabetic kidney disease. *Nat. Rev. Nephrol.* **14**, 291–312 (2018).
12. Szeto, H. H. et al. Protection of mitochondria prevents high-fat diet–induced glomerulopathy and proximal tubular injury. *Kidney Int.* **90**, 997–1011 (2016).
13. Doke, T. et al. NAD+ precursor supplementation prevents mtRNA/RIG-I-dependent inflammation during kidney injury. *Nat. Metab.* **5**, 414–430 (2023).
14. Poyan Mehr, A. et al. De novo NAD+ biosynthetic impairment in acute kidney injury in humans. *Nat. Med.* **24**, 1351–1359 (2018).
15. Chanvillard, L., Tammaro, A. & Sorrentino, V. NAD+ metabolism and interventions in premature renal aging and chronic kidney disease. *Cells* **12**, 21 (2022).
16. Juszczak, F., Arnould, T. & Declèves, A.-E. The role of mitochondrial sirtuins (SIRT3, SIRT4 and SIRT5) in renal cell metabolism: Implication for kidney diseases. *Int. J. Mol. Sci.* **25**, 6936 (2024).
17. Bause, A. S. & Haigis, M. C. SIRT3 regulation of mitochondrial oxidative stress. *Exp. Gerontol.* **48**, 634–639 (2013).
18. Dikalova, A. E. et al. Sirt3 impairment and SOD2 hyperacetylation in vascular oxidative stress and hypertension. *Circ. Res.* **121**, 564–574 (2017).
19. Chen, Y. et al. Tumour suppressor SIRT3 deacetylates and activates manganese superoxide dismutase to scavenge ROS. *EMBO Rep.* **12**, 534–541 (2011).
20. Morevati, M. et al. Roles of NAD+ in acute and chronic kidney diseases. *Int. J. Mol. Sci.* **24**, 137 (2023).
21. Ogura, Y., Kitada, M., Xu, J., Monno, I. & Koya, D. CD38 inhibition by apigenin ameliorates mitochondrial oxidative stress through restoration of the intracellular NAD+/NADH ratio and Sirt3 activity in renal tubular cells in diabetic rats. *Aging* **12**, 11325–11336 (2020).
22. Xie, N. et al. NAD+ metabolism: Pathophysiologic mechanisms and therapeutic potential. *Signal Transduct. Target. Ther.* **5**, 1–37 (2020).
23. Trammell, S. A., Yu, L., Redpath, P., Migaud, M. E. & Brenner, C. Nicotinamide riboside is a major NAD+ precursor vitamin in cow milk. *J. Nutr.* **146**, 957–963 (2016).
24. Belenky, P. et al. Nicotinamide riboside promotes Sir2 silencing and extends lifespan via Nrk and Urh1/Pnp1/Meu1 pathways to NAD+. *Cell* **129**, 473–484 (2007).
25. Bieganowski, P. & Brenner, C. Discoveries of nicotinamide riboside as a nutrient and conserved NRK genes establish a Preiss-Handler independent route to NAD+ in fungi and humans. *Cell* **117**, 495–502 (2004).
26. Trammell, S. A. J. et al. Nicotinamide riboside is uniquely and orally bioavailable in mice and humans. *Nat. Commun.* **7**, 12948 (2016).
27. Yoshino, J., Baur, J. A. & Imai, S. NAD+ intermediates: The biology and therapeutic potential of NMN and NR. *Cell Metab.* **27**, 513–528 (2018).
28. Cantó, C. et al. The NAD+ precursor nicotinamide riboside enhances oxidative metabolism and protects against high-fat diet-induced obesity. *Cell Metab.* **15**, 838–847 (2012).
29. Deji, N. et al. Structural and functional changes in the kidneys of high-fat diet-induced obese mice. *Am. J. Physiol.-Ren. Physiol.* **296**, F118–F126 (2009).
30. Kendrick, A. A. et al. Fatty liver is associated with reduced SIRT3 activity and mitochondrial protein hyperacetylation. *Biochem. J.* **433**, 505–514 (2011).
31. Hirschey, M. D. et al. SIRT3 deficiency and mitochondrial protein hyperacetylation accelerate the development of the metabolic syndrome. *Mol. Cell* **44**, 177–190 (2011).
32. Bhargava, P. & Schnellmann, R. G. Mitochondrial energetics in the kidney. *Nat. Rev. Nephrol.* **13**, 629–646 (2017).
33. Li, Y. et al. BNIP3L/NIX-mediated mitophagy: molecular mechanisms and implications for human disease. *Cell Death Dis.* **13**, 14 (2021).
34. Kim, M.-B. et al. Nicotinamide riboside supplementation exerts an anti–obesity effect and prevents inflammation and fibrosis in white adipose tissue of female diet-induced obesity mice. *J. Nutr. Biochem.* **107**, 109058 (2022).
35. Zhou, A.-J. et al. Long-Term administration of nicotinamide mononucleotide mitigates high-fat-diet-induced physiological decline in aging mice. *J. Nutr.* **S0022–3166**(24), 01094. https://doi.org/10.1016/j.tjnut.2024.10.017 (2024).
36. Morel, J.-D. et al. Mitochondrial and NAD^+ metabolism predict recovery from acute kidney injury in a diverse mouse population. *JCI Insight* **8**(3), e164626 (2023).
37. Yang, S., Gong, W., Wang, Y., Hao, C. & Guan, Y. Unraveling the nexus of NAD+ metabolism and diabetic kidney disease: insights from murine models and human data. *Front. Endocrinol.* **15**, 1384953 (2024).
38. Bignon, Y. et al. Cell stress response impairs de novo NAD^+ biosynthesis in the kidney. *JCI Insight* **7**, e153019 (2022).
39. Guan, Y. et al. Nicotinamide mononucleotide, an NAD+ precursor, rescues age-associated susceptibility to AKI in a sirtuin 1–dependent manner. *J. Am. Soc. Nephrol. JASN* **28**, 2337 (2017).
40. Tran, M. T. et al. PGC1α-dependent NAD biosynthesis links oxidative metabolism to renal protection. *Nature* **531**, 528 (2016).
41. Jia, Y. et al. Nicotinamide mononucleotide attenuates renal interstitial fibrosis after AKI by suppressing tubular DNA damage and senescence. *Front. Physiol.* **12**, 649547 (2021).
42. Zapata-Pérez, R. et al. Reduced nicotinamide mononucleotide is a new and potent NAD^+ precursor in mammalian cells and mice. *FASEB J.* **35**, e21456 (2021).
43. Declèves, A.-E. et al. AMP-activated protein kinase activation ameliorates eicosanoid dysregulation in high-fat-induced kidney disease in mice. *J. Lipid Res.* **60**, 937–952 (2019).
44. Cartwright, D. M. et al. Nicotinamide riboside has minimal impact on energy metabolism in mouse models of mild obesity. *J. Endocrinol.* **251**, 111–123 (2021).
45. Williams, A. S. et al. Nicotinamide riboside supplementation confers marginal metabolic benefits in obese mice without remodeling the muscle acetyl-proteome. *iScience* **25**, 103635 (2022).
46. Pham, T. X. et al. Nicotinamide riboside, an NAD+ precursor, attenuates the development of liver fibrosis in a diet-induced mouse model of liver fibrosis. *Biochimica et Biophysica Acta (BBA)* **1865**, 2451–2463 (2019).
47. Qiu, X., Brown, K., Hirschey, M. D., Verdin, E. & Chen, D. Calorie restriction reduces oxidative stress by SIRT3-mediated SOD2 activation. *Cell Metab.* **12**, 662–667 (2010).
48. Thapa, D. et al. Cardiomyocyte-specific deletion of GCN5L1 in mice restricts mitochondrial protein hyperacetylation in response to a high fat diet. *Sci. Rep.* **10**, 10665 (2020).
49. Annevelink, C. E., Sapp, P. A., Petersen, K. S., Shearer, G. C. & Kris-Etherton, P. M. Diet-derived and diet-related endogenously produced Palmitic Acid: Effects on metabolic regulation and cardiovascular disease risk. *J. Clin. Lipidol.* **17**, 577–586 (2023).

50. Wu, Y. et al. Berberine (BBR) attenuated palmitic acid (PA)-induced Lipotoxicity in human HK-2 cells by promoting peroxisome proliferator-activated receptor a (PPAR-a). *Med. Sci. Monit. Int. Med. J. Exp. Clin. Res.* **25**, 7702 (2019).
51. Liu, T. et al. Palmitic acid-induced podocyte apoptosis via the reactive oxygen species-dependent mitochondrial pathway. *Kidney Blood Press. Res.* **43**, 206–219 (2018).
52. Pierre, L. et al. (2024) AMPK protects proximal tubular epithelial cells from lysosomal dysfunction and dedifferentiation induced by lipotoxicity. *Autophagy* https://doi.org/10.1080/155486272435238 (2024).
53. Fang, E. F. et al. NAD+ replenishment improves lifespan and healthspan in ataxia telangiectasia models via mitophagy and DNA repair. *Cell Metab.* **24**, 566–581 (2016).
54. Schöndorf, D. C. et al. The NAD+ precursor Nicotinamide Riboside rescues mitochondrial defects and neuronal loss in iPSC and fly models of Parkinson's Disease. *Cell Rep.* **23**, 2976–2988 (2018).
55. Fang, E. F. et al. NAD+ augmentation restores mitophagy and limits accelerated aging in Werner syndrome. *Nat. Commun.* **10**, 5284 (2019).
56. Gariani, K. et al. Eliciting the mitochondrial unfolded protein response by nicotinamide adenine dinucleotide repletion reverses fatty liver disease in mice. *Hepatology* **63**, 1190 (2016).
57. Lapatto, H. A. K. et al. Nicotinamide riboside improves muscle mitochondrial biogenesis, satellite cell differentiation, and gut microbiota in a twin study. *Sci. Adv.* **9**, eadd5163 (2023).
58. Luongo, T. S. et al. SLC25A51 is a mammalian mitochondrial NAD+ transporter. *Nature* **588**, 174–179 (2020).
59. Shi, W. et al. High dose of dietary nicotinamide riboside induces glucose intolerance and white adipose tissue dysfunction in mice fed a mildly obesogenic diet. *Nutrients* **11**, 2439 (2019).
60. Shi, W. et al. Effects of a wide range of dietary nicotinamide riboside (NR) concentrations on metabolic flexibility and white adipose tissue (WAT) of mice fed a mildly obesogenic diet. *Mol. Nutr. Food Res.* **61**, 1600878 (2017).
61. Ryu, J.-E. et al. Evaluation of nonalcoholic fatty liver disease in C57BL/6J mice by using MRI and histopathologic analyses. *Comp. Med.* **65**, 409–415 (2015).
62. Journe, F. et al. Steroid-free medium discloses oestrogenic effects of the bisphosphonate clodronate on breast cancer cells. *Br. J. Cancer* **91**, 1703–1710 (2004).

Acknowledgements

This work was supported by Grants from the UMONS Research Institute for Health Sciences and Technology (Belgium), the F.R.S-FNRS (Fonds de la Recherche Scientifique; J004620F), the French Diabetes Society and NARILIS (NAmur Research Institute for LIfe Sciences, Belgium).

Author contributions

Among the authors, FJ and A-ED conceived the experiments; MD, LP, PR, HM, LM, MT and IJ performed the experiments and interpreted the data; FJ oversaw the experiments; MD, LP, TA, A-ED and FJ prepared the manuscript. All authors approved the final version of the manuscript and agree to be accountable for all aspects of the work. All people designated as authors qualify for authorship, and all those who qualify for authorship are listed. All authors have read and agreed to the published version of the manuscript.

Funding

This work was supported by Grants from the UMONS Research Institute for Health Sciences and Technology (Belgium), the F.R.S-FNRS (Fonds de la Recherche Scientifique; J004620F), the French Diabetes Society and NARILIS (NAmur Research Institute for LIfe Sciences, Belgium).

Declarations

Competing interests

The authors declare no competing interests.

Additional information

Supplementary Information The online version contains supplementary material available at https://doi.org/10.1038/s41598-026-46173-x.

Correspondence and requests for materials should be addressed to F.J.

Reprints and permissions information is available at www.nature.com/reprints.

Publisher's note Springer Nature remains neutral with regard to jurisdictional claims in published maps and institutional affiliations.